Handbook of Advanced Ceramics: Materials, Applications, Processing and Properties

Article · January 2003

7 authors, including:

Kenji Uchino
Pennsylvania State University
527 PUBLICATIONS **17,439** CITATIONS

SEE PROFILE

Handbook of Advanced Ceramics
S. Sōmiya *et al.* (Eds.)

4.1 Piezoelectric Ceramics

KENJI UCHINO
International Center for Actuators and Transducers,
134 Materials Research Laboratory, Pennsylvania State University,
University Park, PA 16802-4801, USA

Certain materials produce electric charges on their surfaces as a consequence of applying mechanical stress. The induced charges are proportional to the mechanical stress. This is called the direct piezoelectric effect and was discovered in quartz by Piere and Jacques Curie in 1880. Materials showing this phenomenon also conversely have a geometric strain proportional to an applied electric field. This is the converse piezoelectric effect. The root of the word "piezo" means "pressure"; hence the original meaning of the word piezoelectricity implied "pressure electricity".

Piezoelectricity is extensively utilized in the fabrication of various devices such as transducers, actuators, surface acoustic wave devices, frequency control and so on. In this chapter we describe the piezoelectric materials that are used, and various potential applications of piezoelectric materials [1–4].

4.1.1 PIEZOELECTRIC MATERIALS AND PROPERTIES

4.1.1.1 PIEZOELECTRIC FIGURES OF MERIT

There are five important figures of merit in piezoelectrics: the piezoelectric strain constant d, the piezoelectric voltage constant g, the electromechanical coupling factor k, the mechanical quality factor Q_M, and the acoustic impedance Z. These figures of merit are considered in this section.

4.1.1.1.1 Piezoelectric Strain Constant *d*

The magnitude of the induced strain x by an external electric field E is represented by this figure of merit (an important figure of merit for actuator applications):

$$x = dE. \tag{1}$$

4.1.1.1.2 Piezoelectric Voltage Constant *g*

The induced electric field E is related to an external stress X through the piezoelectric voltage constant g (an important figure of merit for sensor applications):

$$E = gX. \tag{2}$$

Taking into account the relation, $P = dX$, we obtain an important relation between g and d:

$$g = d/\varepsilon_0\varepsilon \quad (\varepsilon\text{: permittivity}) \tag{3}$$

4.1.1.1.3 Electromechanical Coupling Factor *k*

The terms, electromechanical coupling factor, energy transmission coefficient, and efficiency are sometimes confused [5]. All are related to the conversion rate between electrical energy and mechanical energy, but their definitions are different [6].

(a) *The electromechanical coupling factor k*

$$k^2 = (\text{stored mechanical energy/input electrical energy}) \tag{4}$$

or

$$k^2 = (\text{stored electrical energy/input mechanical energy}) \tag{5}$$

Let us calculate Eq. 4, when an electric field E is applied to a piezoelectric material. Since the input electrical energy is $(1/2)\varepsilon_0\varepsilon E^2$ per unit volume and the stored mechanical energy per unit volume under zero external stress is given by $(1/2)x^2/s = (1/2)(dE)^2/s$, k^2 can be calculated as

$$\begin{aligned} k^2 &= \left[(1/2)(dE)^2/s\right] \Big/ \left[(1/2)\varepsilon_0\varepsilon E^2\right] \\ &= d^2/\varepsilon_0\varepsilon \cdot s. \end{aligned} \tag{6}$$

(b) *The energy transmission coefficient* λ_{max}

Not all the stored energy can be actually used, and the actual work done depends on the mechanical load. With zero mechanical load or a complete clamp (no strain) zero output work is done.

$$\lambda_{max} = (\text{output mechanical energy/input electrical energy})_{max} \tag{7}$$

or

$$\lambda_{max} = (\text{output electrical energy/input mechanical energy})_{max} \tag{8}$$

Let us consider the case where an electric field E is applied to a piezoelectric under constant external stress X (<0, because a compressive stress is necessary to work to the outside). As shown in Figure 4.1.1, the output work can be calculated as

$$\int (-X)\,\mathrm{d}x = -(dE + sX)X, \tag{9}$$

while the input electrical energy is given by

$$\int E\,\mathrm{d}P = (\varepsilon_0\varepsilon E + dX)E. \tag{10}$$

We need to choose a proper load to maximize the energy transmission coefficient. From the maximum condition of

$$\lambda = -(dE + sX)X/(\varepsilon_0\varepsilon E + dX)E, \tag{11}$$

we can obtain

$$\begin{aligned}\lambda_{\max} &= [(1/k) - \sqrt{(1/k^2) - 1}]^2 \\ &= [(1/k) + \sqrt{(1/k^2) - 1}]^{-2}\end{aligned} \tag{12}$$

Notice that

$$k^2/4 < \lambda_{\max} < k^2/2 \tag{13}$$

depending on the k value. For a small k, $\lambda_{\max} = k^2/4$, and for a large k, $\lambda_{\max} = k^2/2$.

It is also worth noting that the maximum condition stated above does not agree with the condition which provides the maximum output mechanical energy. The maximum output energy can be obtained when the load is half of the maximum generative stress: $-(dE - s(dE/2s))(-dE/2s) = (dE)^2/4s$. In this case, since the input electrical energy is given by $(\varepsilon_0\varepsilon E + d(-dE/2s))E$,

$$\lambda = 1/2[(2/k^2) - 1], \tag{14}$$

which is close to the value $\lambda_{\max}$, but has a different value that is predicted theoretically.

(c) *The efficiency* η

$$\eta = (\text{output mechanical energy})/(\text{consumed electrical energy}) \tag{15}$$

or

$$\eta = (\text{output electrical energy})/(\text{consumed mechanical energy}). \tag{16}$$

In a work cycle (e.g. an electric field cycle), the input electrical energy is transformed partially into mechanical energy and the remaining is stored

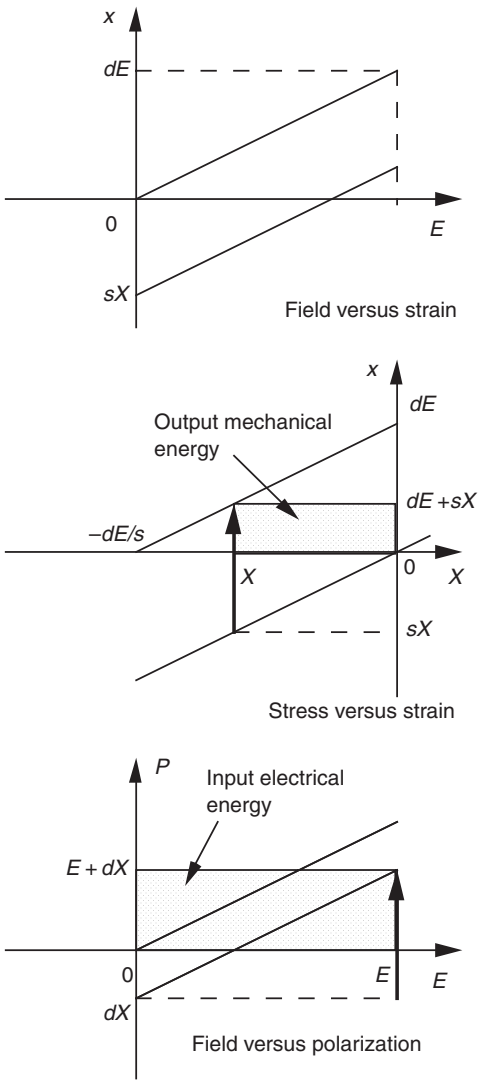

FIGURE 4.1.1 Calculation of the input electrical and output mechanical energy.

as electrical energy (electrostatic energy like a capacitor) in an actuator. In this way, the ineffective energy can be returned to the power source, leading to near 100% efficiency, if the loss is small. Typical values of dielectric loss in PZT are about 1–3%.

4.1.1.1.4 Mechanical Quality Factor Q_M

The mechanical quality factor, Q_M, is a parameter that characterizes the sharpness of the electromechanical resonance spectrum. When the motional admittance Y_m is plotted around the resonance frequency ω_0, the mechanical quality factor Q_M is defined with respect to the full width at $Y_m/\sqrt{2}[2\Delta\omega]$ as:

$$Q_M = \omega_0/2\Delta\omega. \tag{17}$$

Also note that Q_M^{-1} is equal to the mechanical loss ($\tan\delta_m$). The Q_M value is very important in evaluating the magnitude of the resonant strain. The vibration amplitude at an off-resonance frequency (dEL, L: length of the sample) is amplified by a factor proportional to Q_M at the resonance frequency. For a longitudinally vibration rectangular plate through d_{31}, the maximum displacement is given by $(8/\pi^2)Q_M d_{31} EL$.

4.1.1.1.5 Acoustic Impedance Z

The acoustic impedance Z is a parameter used for evaluating the acoustic energy transfer between two materials. It is defined, in general, by

$$Z^2 = (\text{pressure/volume velocity}). \tag{18}$$

In a solid material,

$$Z = \sqrt{\rho c}, \tag{19}$$

where ρ is the density and c the elastic stiffness of the material.

In more advanced discussions, there are three kinds of impedances; specific acoustic impedance (pressure/particle speed), acoustic impedance (pressure/volume speed) and radiation impedance (force/speed). See Ref. [6] for the details.

4.1.1.2 Piezoelectric Materials [7]

This section summarizes the current status of piezoelectric materials: single-crystal materials, piezoceramics, piezopolymers, piezocomposites and piezofilms. Table 4.1.1 shows the material parameters of some of the piezoelectric materials [8].

4.1.1.2.1 Single Crystals

Although piezoelectric ceramics are widely used for a large number of applications, single-crystal materials retain their utility, being essential for applications

TABLE 4.1.1 Piezoelectric Properties of Representative Piezoelectric Materials [7, 8]

Parameter	Quartz	$BaTiO_3$	PZT 4	PST5H	(Pb, Sm)TiO_3	PVDF-TrFE
d_{33} (pC/N)	2.3	190	289	593	65	33
g_{33} (10^{-3} V m/N)	57.8	12.6	26.1	19.7	42	380
k_t	0.09	0.38	0.51	0.50	0.50	0.30
k_p	—	0.33	0.58	0.65	0.03	—
$\varepsilon_3^T/\varepsilon_0$	5	1700	1300	3400	175	6
Q_M	$>10^5$	—	500	65	900	3–10
T_C (°C)	—	120	328	193	355	—

such as frequency stabilized oscillators and surface acoustic devices. The most popular single-crystal piezoelectric materials are quartz, lithium niobate ($LiNbO_3$), and lithium tantalate ($LiTaO_3$). The single crystals are anisotropic, exhibiting different material properties depending on the cut of the materials and the direction of bulk or surface wave propagation.

Quartz is a well-known piezoelectric material. α-Quartz belongs to the triclinic crystal system with point group 32 and has a phase transition at 537°C to its β-form, which is not piezoelectric. Quartz has a cut with a zero temperature coefficient. For instance, quartz oscillators, operated in the thickness shear mode of the AT-cut, are used extensively for clock sources in computers, frequency stabilized ones in TVs and VCRs. On the other hand, an ST-cut quartz substrate with X-propagation has a zero temperature coefficient for surface acoustic wave and so is used for SAW devices with high-stabilized frequencies. The another distinguished characteristic of quartz is an extremely high mechanical quality factor $Q_M > 10^5$.

$LiNbO_3$ and $LiTaO_3$ belong to an isomorphous crystal system and are composed of oxygen octahedron. The Curie temperatures of $LiNbO_3$ and $LiTaO_3$ are 1210 and 660°C, respectively. The crystal symmetry of the ferroelectric phase of these single crystals is 3*m* and the polarization direction is along *c*-axis. These materials have high electromechanical coupling coefficients for surface acoustic wave. In addition, large single crystals can easily be obtained from their melt using the conventional Czochralski technique. Thus both materials occupy very important positions in the surface acoustic wave (SAW) device application field.

4.1.1.2.2 Polycrystalline Materials

Barium titanate ($BaTiO_3$) is one of the most thoroughly studied and most widely used piezoelectric materials. Just below the Curie temperature (120°C), the vector of the spontaneous polarization points in the [001] direction

(tetragonal phase), below 5°C it reorients in the [011] (orthrhombic phase) and below −90°C in the [111] direction (rhombohedral phase). The dielectric and piezoelectric properties of ferroelectric ceramic $BaTiO_3$ can be affected by its own stoichiometry, microstructure, and by dopants entering onto the A or B site in solid solution. Modified ceramic $BaTiO_3$ with dopants such as Pb or Ca ions have been developed to stabilize the tetragonal phase over a wider temperature range and are used as commercial piezoelectric materials. The initial application was for Langevin-type piezoelectric vibrators.

Piezoelectric $Pb(Ti,Zr)O_3$ solid solutions (PZT) ceramics have been widely used because of their superior piezoelectric properties. The phase diagram for the PZT system ($PbZr_xTi_{1-x}O_3$) is shown in Figure 4.1.2. The crystalline symmetry of this solid-solution system is determined by the Zr content. Lead titanate also has a tetragonal ferroelectric phase of perovskite structure. With increasing Zr content, x, the tetragonal distortion decreases and at $x > 0.52$ the structure changes from the tetragonal 4*mm* phase to another ferroelectric phase of rhombohedral 3*m* symmetry. The line dividing these two phases is called the *morphotropic phase boundary* (MPB). The boundary composition is considered to have both tetragonal and rhombohedral phases coexisting together. Figure 4.1.3 shows the dependence of several piezoelectric d constants on composition near the MPB. The d constants have their highest values near

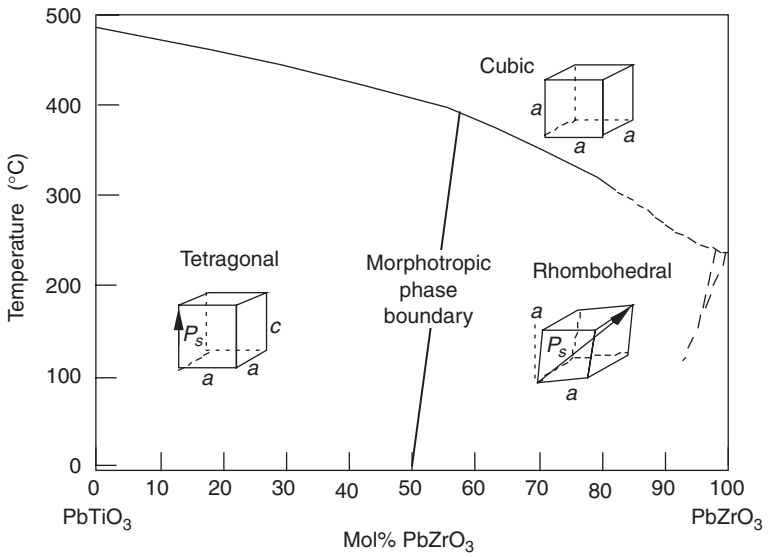

FIGURE 4.1.2 Phase diagram of lead zirconate titanate (PZT).

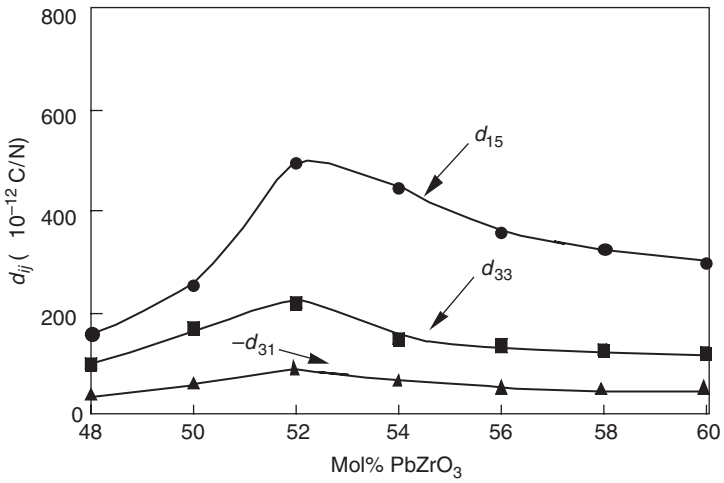

FIGURE 4.1.3 Dependence of several d constants on composition near the morphotropic phase boundary in the PZT system.

the MPB. This enhancement in piezoelectric effect is attributed to the increased ease of reorientation of the polarization under an applied electric field.

Doping the PZT material with donor or acceptor ions changes its properties dramatically. Donor doping with ions such as Nb^{5+} or Ta^{5+} provides soft PZTs, like PZT-5, because of the facility of domain motion due to the resulting Pb-vacancies. On the other hand, acceptor doping with Fe^{3+} or Sc^{3+} leads to hard PZTs, such as PZT-8, because the oxygen vacancies will pin domain wall motion.

Subsequently, PZT in ternary solid solution with another perovskite phase has been investigated intensively. Examples of these ternary compositions are: PZTs in solid solution with $Pb(Mg_{1/3}Nb_{2/3})O_3$, $Pb(Mn_{1/3}Sb_{2/3})O_3$, $Pb(Co_{1/3}Nb_{2/3})O_3$, $Pb(Mn_{1/3}Nb_{2/3})O_3$, $Pb(Ni_{1/3}Nb_{2/3})O_3$, $Pb(Sb_{1/2}Sn_{1/2})O_3$, $Pb(Co_{1/2}W_{1/2})O_3$, $Pb(Mg_{1/2}W_{1/2})O_3$, all of which are patented by different companies.

The end member of PZT, lead titanate has a large crystal distortion. $PbTiO_3$ has a tetragonal structure at room temperature with its tetragonality $c/a = 1.063$. The Curie temperature is 490°C. Densely sintered $PbTiO_3$ ceramics cannot be obtained easily, because they break up into a powder when cooled through the Curie temperature due to the large spontaneous strain. Lead titanate ceramics modified by adding a small amount of additives exhibit a high piezoelectric anisotropy. Either (Pb, Sm)TiO_3 [9] or (Pb, Ca)TiO_3 [10] exhibits an extremely low planar coupling, that is, a large k_t/k_p ratio. Here,

k_t and k_p are thickness-extensional and planar electromechanical coupling factors, respectively. Since these transducers can generate purely longitudinal waves through k_t associated with no transverse waves through k_{31}, clear ultrasonic imaging is expected without "ghost" caused by the transverse wave. (Pb,Nd)(Ti,Mn,In)O_3 ceramics with a zero temperature coefficient of SAW delay have been developed as superior substrate materials for SAW device applications [11].

4.1.1.2.3 Relaxor Ferroelectrics

Relaxor ferroelectrics can be prepared either in polycrystalline form or as single crystals. They differ from the previously mentioned normal ferroelectrics in that they exhibit a broad phase transition from the paraelectric to ferroelectric state, a strong frequency dependence of the dielectric constant (i.e. dielectric relaxation) and a weak remanent polarization. Lead-based relaxor materials have complex disordered perovskite structures.

Relaxor-type electrostrictive materials, such as those from the lead magnesium niobate–lead titanate, $Pb(Mg_{1/3}Nb_{2/3})O_3$–$PbTiO_3$ (or PMN–PT), solid solution are highly suitable for actuator applications. This relaxor ferroelectric also exhibits an induced piezoelectric effect. That is, the electromechanical coupling factor k_t varies with the applied DC bias field. As the DC bias field increases, the coupling increases and saturates. Since this behavior is reproducible, these materials can be applied as ultrasonic transducers which are tunable by the bias field [12].

Recently, single-crystal relaxor ferroelectrics with the MPB composition have been developed which show tremendous promise as ultrasonic transducers and electromechanical actuators. Single crystals of $Pb(Mg_{1/3}Nb_{2/3})O_3$ (PMN), $Pb(Zn_{1/3}Nb_{2/3})O_3$ (PZN) and binary systems of these materials combined with $PbTiO_3$ (PMN–PT and PZN–PT) exhibit extremely large electromechanical coupling factors [13, 14]. Large coupling coefficients and large piezoelectric constants have been found for crystals from the morphotropic phase boundaries of these solid solutions. PZN–8% PT single crystals were found to possess a high k_{33} value of 0.94 for the (001) crystal cuts; this is very high compared to the k_{33} of conventional PZT ceramics of around 0.70–0.80.

4.1.1.2.4 Polymers

Polyvinylidene difluoride, PVDF or PVF2, is piezoelectric when stretched during fabrication. Thin sheets of the cast polymer are then drawn and stretched in the plane of the sheet, in at least one direction, and frequently also in the perpendicular direction, to transform the material to its microscopically polar phase. Crystallization from the melt forms the non-polar α-phase, which can be

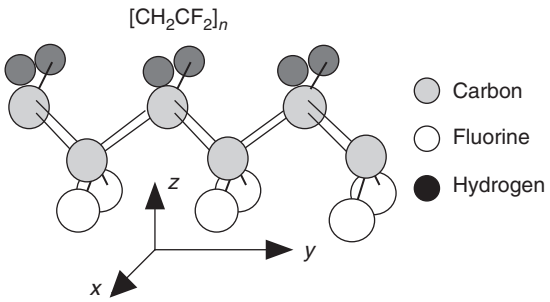

FIGURE 4.1.4 Structure of polyvinylidene diflouride (PVDF).

converted into the polar β-phase by a uniaxial or biaxial drawing operation; the resulting dipoles are then reoriented through electric poling (see Figure 4.1.4).

Large sheets can be manufactured and thermally formed into complex shapes. The copolymerization of vinilydene difluoride with trifluoroethylene (TrFE) results in a random copolymer (PVDF–TrFE) with a stable, polar β-phase. This polymer need not be stretched; it can be poled directly as formed. A thickness-mode coupling coefficient of 0.30 has been reported. Piezoelectric polymers have the following characteristics: (a) small piezoelectric *d* constants (for actuators) and large *g* constants (for sensors); (b) light weight and soft elasticity, leading to good acoustic impedance matching with water or the human body; and (c) a low mechanical quality factor Q_M, allowing for a broad resonance band width. Such piezoelectric polymers are used for directional microphones and ultrasonic hydrophones.

4.1.1.2.5 Composites

Piezocomposites comprised of a piezoelectric ceramic and a polymer phase are promising materials because of their excellent and readily tailored properties. The geometry for two-phase composites can be classified according to the dimensional connectivity of each phase into 10 structures; 0–0, 0–1, 0–2, 0–3, 1–1, 1–2, 1–3, 2–2, 2–3 and 3–3 [15]. A 1–3 piezocomposite, such as the PZT-rod/polymer composite is a most promising candidate. The advantages of this composite are high coupling factors, low acoustic impedance, good matching to water or human tissue, mechanical flexibility, broad bandwidth in combination with a low mechanical quality factor and the possibility of making undiced arrays by structuring the electrodes. The thickness-mode electromechanical coupling of the composite can exceed the k_t (0.40–0.50) of the constituent ceramic, approaching almost the value of the rod-mode electromechanical coupling, k_{33} (0.70–0.80) of that ceramic [16]. Acoustic impedance is the square

root of the product of its density and elastic stiffness. The acoustic match to tissue or water (1.5 Mrayls) of the typical piezoceramics (20–30 Mrayls) is significantly improved by forming a composite structure, that is, by replacing some of the heavy, stiff ceramic with a light, soft polymer. Piezoelectric composite materials are especially useful for underwater sonar and medical diagnostic ultrasonic transducer applications.

4.1.1.2.6 Thin Films

Both zinc oxide (ZnO) and aluminum nitride (AlN) are simple binary compounds with a Wurtzite-type structure, which can be sputter-deposited as a *c*-axis oriented thin film on a variety of substrates. ZnO has large piezoelectric coupling and thin films of this material are widely used in bulk acoustic and surface acoustic wave devices. The fabrication of highly oriented (along the *c*-axis) ZnO films have been studied and developed extensively. The performance of ZnO devices is limited, however, due to their low piezoelectric coupling (20–30%). PZT thin films are expected to exhibit higher piezoelectric properties. At present the growth of PZT thin films is being carried out for use in microtransducers and microactuators.

4.1.2 PRESSURE SENSORS/ACCELEROMETERS/ GYROSCOPES

One of the very basic applications of piezoelectric ceramics is a gas igniter. The very high voltage generated in a piezoelectric ceramic under applied mechanical stress can cause sparking and ignite the gas (Fig. 4.1.5). There are two means to apply the mechanical force, either by a rapid, pulsed application or by a more gradual, continuous increase.

Piezoelectric ceramics can be employed as stress sensors and acceleration sensors, because of the *direct piezoelectric effect*. Figure 4.1.6 shows a three-dimensional (3D) stress sensor designed by Kistler. By combining an appropriate number of quartz crystal plates (extensional and shear types), the multilayer device can detect 3D stresses [17].

Figure 4.1.7 shows a cylindrical gyroscope commercialized by Tokin (Japan) [18]. The cylinder has six divided electrodes, one pair of which are used to excite the fundamental bending vibration mode, while the other two pairs are used to detect the acceleration. When the rotational acceleration is applied about the axis of this gyro, the voltage generated on the electrodes is modulated by the *Coriolis force*. By subtracting the signals between the two sensor electrode pairs, a voltage directly proportional to the acceleration can be obtained.

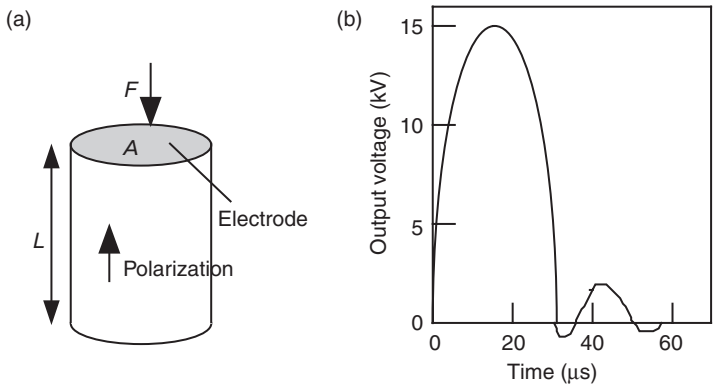

FIGURE 4.1.5 (a) Gas igniter and (b) output voltage.

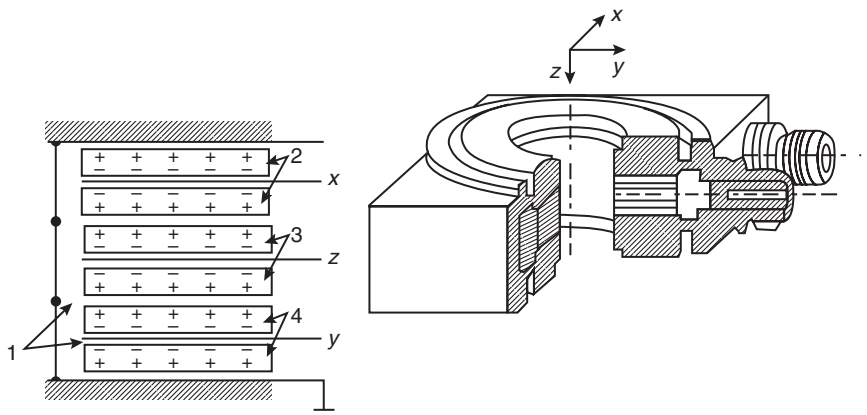

FIGURE 4.1.6 3D stress sensor (by Kistler).

The *converse electrostrictive effect*—the stress dependence of the permittivity—is also used in stress sensors [19]. A bimorph structure provides superior stress sensitivity and temperature stability. A measuring system with a bimorph structure, which subtracts the static capacitances of two dielectric ceramic plates, has been proposed [19]. The capacitance changes of the top and bottom plates have opposite signs for uniaxial stress and the same sign for temperature deviation. The response speed is limited by the capacitance measuring frequency to about 1 kHz. Unlike piezoelectric sensors, electrostrictive sensors are effective in the low-frequency range, especially DC.

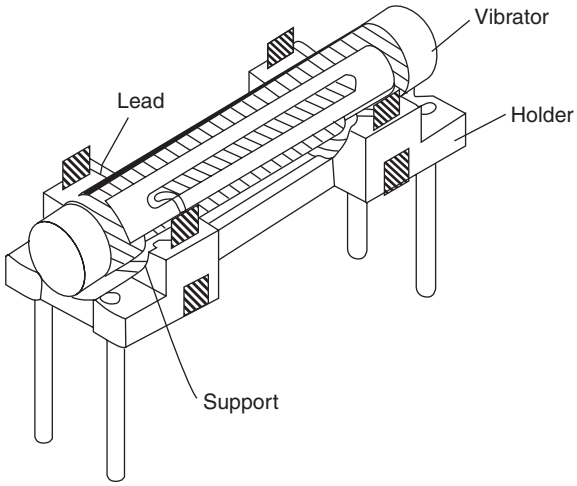

FIGURE 4.1.7 Cylindrical gyroscope (by Tokin).

4.1.3 PIEZOELECTRIC VIBRATORS/ULTRASONIC TRANSDUCERS

4.1.3.1 Piezoelectric Resonance

4.1.3.1.1 The Piezoelectric Equations

When an electric field is applied to a piezoelectric material, deformation (ΔL) or strain ($\Delta L/L$) arises. When the field is alternating, mechanical vibration is caused, and if the drive frequency is adjusted to a mechanical resonance frequency of the device, large resonating strain is generated. This phenomenon can be understood as a strain magnification due to accumulating input energy, and is called *piezoelectric resonance*. Piezoelectric resonance is very useful for realizing energy trap devices, actuators, etc. The theoretical treatment is as follows.

If the applied electric field and the generated stress are not large, the stress X and the dielectric displacement D can be represented by the following equations:

$$x_i = s_{ij}^E X_j + d_{mi} E_m, \tag{20}$$

$$D_m = d_{mi} X_i + \varepsilon_{mk}^X E_k \tag{21}$$

where $i, j = 1, 2, \ldots, 6;\ m, k = 1, 2, 3$.

These are called the *piezoelectric equations*. The number of independent parameters for the lowest symmetry trigonal crystal are 21 for s_{ij}^E, 18 for d_{mi}

and 6 for ε^X_{mk}. The number of independent parameters decreases with increasing crystallographic symmetry. Concerning the polycrystalline ceramics, the poled axis is usually denoted as the z-axis and the ceramic is isotropic with respect to this z-axis (Curie group $C_{\infty v}(\infty m)$). The number of non-zero matrix elements in this case is 10 ($s^E_{11}, s^E_{12}, s^E_{13}, s^E_{33}, s^E_{44}, d_{31}, d_{33}, d_{15}, \varepsilon^X_{11}$, and ε^X_{33}).

4.1.3.1.2 Electromechanical Coupling Factor

Next let us introduce the *electromechanical coupling factor* k, which corresponds to the rate of electromechanical transduction. The internal energy U of a piezoelectric vibrator is given by summation of the mechanical energy U_M ($= \int x\,dX$) and the electrical energy U_E ($= \int D\,dE$). U is calculated as follows, when linear relations Eqs 20 and 21 are applicable:

$$U = U_M + U_E = \left[\frac{1}{2}\sum_{i,j} s^E_{ij} X_j X_i + \frac{1}{2}\sum_{m,i} d_{mi} E_m X_i\right] + \left[\frac{1}{2}\sum_{i,j} d_{mi} X_i E_m + \frac{1}{2}\sum_{k,m} \varepsilon^X_{mk} E_k E_m\right]. \quad (22)$$

The s and E terms represent purely mechanical and electrical energies (U_{MM} and U_{EE}), respectively, and the d term denotes the energy transduced from electrical to mechanical energy or vice versa through the piezoelectric effect. The coupling factor k is defined by:

$$k = U_{ME}/\sqrt{U_{MM} \cdot U_{EE}}. \quad (23)$$

The k value varies with the vibrational mode (even in the same ceramic sample), and can have a positive or negative value. Note that this definition is equivalent to the definition provided in section on "Piesoelectric figures of merit":

$$k^2 = \text{(stored mechanical energy/input electrical energy)}$$

or

$$k^2 = \text{(stored electrical energy/input mechanical energy)}.$$

4.1.3.1.3 Longitudinal Vibration Mode

Let us consider the longitudinal mechanical vibration of a piezoceramic plate through the transverse piezoelectric effect (d_{31}) as shown in Figure 4.1.8. If the polarization is in the z-direction and x–y planes are the planes of the electrodes,

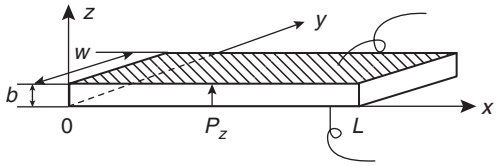

FIGURE 4.1.8 Longitudinal vibration through the transverse piezoelectric effect (d_{31}) in a rectangular plate.

the extentional vibration in the x-direction is represented by the following dynamic equation:

$$\rho(\partial^2 u/\partial t^2) = F = (\partial X_{11}/\partial x) + (\partial X_{12}/\partial y) + (\partial X_{13}/\partial z), \tag{24}$$

where u is the displacement of the small volume element in the ceramic plate in the x-direction. The relations between stress, electric field (only E_z exists) and the induced strain are given by:

$$\begin{aligned}
x_1 &= s_{11}^E X_1 + s_{12}^E X_2 + s_{13}^E X_3 + d_{31} E_z, \\
x_2 &= s_{12}^E X_1 + s_{11}^E X_2 + s_{13}^E X_3 + d_{31} E_z, \\
x_3 &= s_{13}^E X_1 + s_{13}^E X_2 + s_{33}^E X_3 + d_{33} E_z, \\
x_4 &= s_{44}^E X_4, \\
x_5 &= s_{44}^E X_5, \\
x_6 &= 2(s_{11}^E - s_{12}^E) X_6.
\end{aligned} \tag{25}$$

When the plate is very long and thin, X_2 and X_3 may be set equal to zero through the plate. Since shear stress will not be generated by the electric field E_z, Eq. 25 is reduced to:

$$X_1 = x_1/s_{11}^E - (d_{31}/s_{11}^E)E_z. \tag{26}$$

Introducing Eq. 26 into Eq. 24, and allowing for $x_1 = \partial u/\partial x$ and $\partial E_z/\partial x = 0$ (due to the equal potential on each electrode), leads to a harmonic vibration equation:

$$-\omega^2 \rho s_{11}^E u = \partial^2 u/\partial x^2. \tag{27}$$

Here, ω is the angular frequency of the drive field, and ρ is the density. Substituting a general solution $u = u_1(x)e^{j\omega t} + u_2(x)e^{-j\omega t}$ into Eq. 26, and with the boundary condition $X_1 = 0$ at $x = 0$ and L (sample length), the following solution can be obtained:

$$\partial u/\partial x = x_1 = d_{31} E_z[\sin \omega(L - x)/v + \sin(\omega x/v)/\sin(\omega L/v). \tag{28}$$

Here, v is the *sound velocity* in the piezoceramic which is given by

$$v = 1/\sqrt{\rho s_{11}^E}. \tag{29}$$

When the specimen is utilized as an electrical component such as a filter or a vibrator, the electrical impedance [(applied voltage/induced current) ratio] plays an important role. The current flow into the specimen is described by the surface charge increment, $\partial D_3/\partial t$, and the total current is given by:

$$i = j\omega w \int_0^L D_3 \, \mathrm{d}x = j\omega w \int_0^L [(\varepsilon_{33}^X - d_{31}^2/s_{11}^E)E_z + (d_{31}/s_{11}^E)x_1] \, \mathrm{d}x. \tag{30}$$

Using Eq 28, the admittance for the mechanically free sample is calculated to be:

$$\begin{aligned}(1/Z) &= (i/V) = (i/E_z t) \\ &= (j\omega wL/t)\varepsilon_{33}^{\mathrm{LC}}[1 + (d_{31}^2/\varepsilon_{33}^{\mathrm{LC}} s_{11}^E)(\tan(\omega L/2v)/(\omega L/2v)],\end{aligned} \tag{31}$$

where w is the width, L the length, t the thickness of the sample, and V the applied voltage. $\varepsilon_{33}^{\mathrm{LC}}$ is the permittivity in a longitudinally clamped sample, which is given by

$$\varepsilon_{33}^{\mathrm{LC}} = \varepsilon_{33}^X - (d_{31}^2/s_{11}^E). \tag{32}$$

The piezoelectric resonance is achieved where the admittance becomes infinite or the impedance is zero. The resonance frequency f_{R} is calculated from Eq. 31, and the fundamental frequency is given by

$$f_{\mathrm{R}} = v/2L = 1/(2L\sqrt{\rho s_{11}^E}). \tag{33}$$

On the other hand, the antiresonance state is generated for zero admittance or infinite impedance:

$$(\omega_{\mathrm{A}} L/2v) \cot(\omega_{\mathrm{A}} L/2v) = -d_{31}^2/\varepsilon_{33}^{\mathrm{LC}} s_{11}^E = -k_{31}^2/(1 - k_{31}^2). \tag{34}$$

The final transformation is provided by the definition,

$$k_{31} = d_{31}/\sqrt{s_{11}^E \varepsilon_{33}^X}. \tag{35}$$

The resonance and antiresonance states are described by the following intuitive model. In a high electromechanical coupling material with k almost equal to 1, the resonance or antiresonance states appear for $\tan(\omega L/2v) = \infty$ or 0 [i.e. $\omega L/2v = (m - 1/2)\pi$ or $m\pi$ (m: integer)], respectively. The strain amplitude x_1 distribution for each state (calculated using Eq. 28) is illustrated in

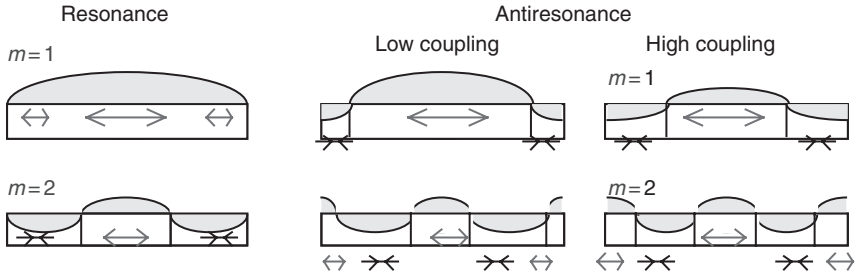

FIGURE 4.1.9 Strain generation in the resonant or antiresonant state.

Figure 4.1.9. In the resonance state, large strain amplitudes and large capacitance changes (called *motional capacitance*) are induced, and the current can easily flow into the device. On the other hand, at antiresonance, the strain induced in the device compensates completely, resulting in no capacitance change, and the current cannot flow easily into the sample. Thus, for a high k material the first antiresonance frequency f_A should be twice as large as the first resonance frequency f_R.

In a typical case, where $k_{31} = 0.3$, the antiresonance state varies from the previously mentioned mode and becomes closer to the resonance mode. The low-coupling material exhibits an antiresonance mode where capacitance change due to the size change is compensated completely by the current required to charge up the static capacitance (called *damped capacitance*). Thus, the antiresonance frequency f_A will approach the resonance frequency f_R.

The general processes for calculating the electromechanical parameters (k_{31}, d_{31}, s_{11}^E, and ε_{33}^X) are described below:

1. The sound velocity v in the specimen is obtained from the resonance frequency f_R (refer to Figure 4.1.10), using Eq. 33.
2. Knowing the density ρ, the elastic compliance s_{11}^E can be calculated.
3. The electromechanical coupling factor k_{31} is calculated from the v value and the antiresonance frequency f_A through Eq. 34. Especially in low-coupling piezoelectric materials, the following approximate equation is available:

$$k_{31}^2/(1 - k_{31}^2) = (\pi^2/4)(\Delta f/f_R) \quad (\Delta f = f_A - f_R) \tag{36}$$

4. Knowing the permittivity ε_{33}^X, the d_{31} is calculated through Eq. 35.

Figure 4.1.10 shows observed impedance curves for a typical k material (PZT 5H, $k_{33} = 0.70$) and a high-k material (PZN–PT single crystal, $k_{33} = 0.90$). Note a large separation between the resonance and antiresonance peaks in the high-k material, leading to the condition $f_A = 2f_R$.

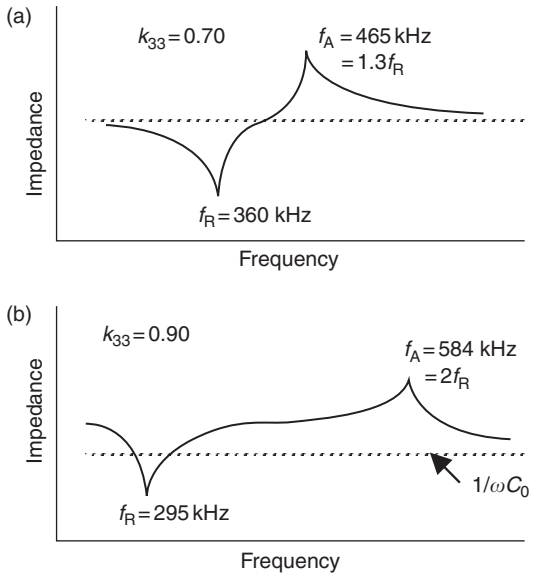

FIGURE 4.1.10 (a) Impedance curves for a reasonable k material (PZT 5H, $k_{33} = 0.70$); and (b) a high-k material (PZN–PT single crystal, $k_{33} = 0.90$).

4.1.3.2 Equivalent Circuits of Piezoelectric Vibrators

The *equivalent circuit* for the piezoelectric acuator is represented by a combination of L, C and R. Figure 4.1.11a shows an equivalent circuit for the resonance state, which has a very low impedance. C_d corresponds to the electrostatic capacitance, and the components L_A and C_A in a series resonance circuit are related to the piezoelectric motion. For example, in the case of the longitudinal vibration of the above rectangular plate through d_{31}, these components are represented by

$$L_A = (\rho/8)(Lb/w)(s_{11}^{E2}/d_{31}^2), \tag{37}$$

$$C_A = (8/\pi^2)(Lw/b)(d_{31}^2/s_{11}^E). \tag{38}$$

The component R_A corresponds to the mechanical loss.

In contrast, the equivalent circuit for the antiresonance state of the same actuator is shown in Figure 4.1.11b, which has high impedance.

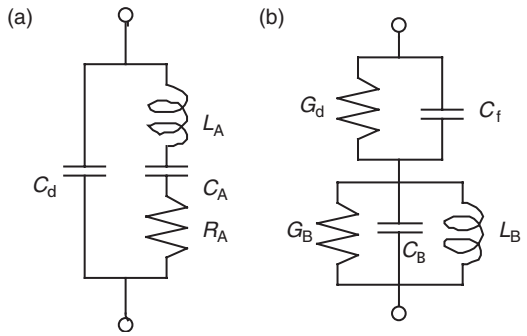

FIGURE 4.1.11 Equivalent circuit of a piezoelectric device for: (a) the resonance: and (b) the antiresonance states.

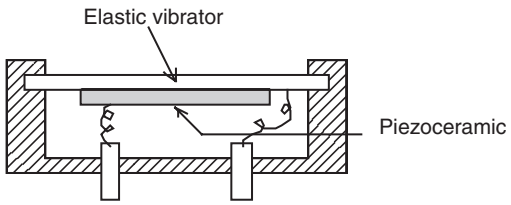

FIGURE 4.1.12 Piezoelectric buzzer.

4.1.3.3 PIEZOELECTRIC VIBRATORS

In the use of mechanical vibration devices such as filters or oscillators, the size and shape of a device are very important, and both the vibrational mode and the ceramic material must be considered. The resonance frequency of the bending mode in a centimeter-size sample ranges from 100 to 1000 Hz, which is much lower than that of the thickness mode (100 kHz). For these vibrator applications the piezoceramic should have a high mechanical quality factor (Q_M) rather than a large piezoelectric coefficient d; that is, hard piezoelectric ceramics are preferable.

For speakers or buzzers, audible by humans, devices with a rather low resonance frequency are used (kilohertz range). Examples are a bimorph consisting of two piezoceramic plates bonded together, and a piezoelectric fork consisting of a piezodevice and a metal fork. A piezoelectric buzzer is shown in Figure 4.1.12, which has merits such as high electric power efficiency, compact size and long life.

4.1.3.4 ULTRASONIC TRANSDUCERS

Ultrasonic waves are now used in various fields. The sound source is made from piezoelectric ceramics as well as magnetostrictive materials. Piezoceramics are generally superior in efficiency and in size to magnetostrictive materials. In particular, hard piezoelectric materials with a high Q_M are preferable. A liquid medium is usually used for sound energy transfer. Ultrasonic washers, ultrasonic microphones for short-distance remote control and underwater detection, such as sonar and fish finding, and non-destructive testing are typical applications. Ultrasonic scanning detectors are useful in medical electronics for clinical applications ranging from diagnosis to therapy and surgery.

One of the most important applications is based on ultrasonic echo field [20, 21]. Ultrasonic transducers convert electrical energy into mechanical form when generating an acoustic pulse and convert mechanical energy into an electrical signal when detecting its echo. The transmitted waves propagate into a body and echoes are generated which travel back to be received by the same transducer. These echoes vary in intensity according to the type of tissue or body structure, thereby creating images. An ultrasonic image represents the mechanical properties of the tissue, such as density and elasticity. We can recognize anatomical structures in an ultrasonic image since the organ boundaries and fluid-to-tissue interfaces are easily discerned. The ultrasonic imaging process can also be done in real time. This means we can follow rapidly moving structures such as the heart without motion distortion. In addition, ultrasound is one of the safest diagnostic imaging techniques. It does not use ionizing radiation like *X*-rays and thus is routinely used for fetal and obstetrical imaging. Useful areas for ultrasonic imaging include cardiac structures, the vascular systems, the fetus and abdominal organs such as liver and kidney. In brief, it is possible to see inside the human body without breaking the skin by using a beam of ultrasound.

Figure 4.1.13 shows the basic ultrasonic transducer geometry. The transducer is mainly composed of matching, piezoelectric material and backing layers [22]. One or more matching layers are used to increase sound transmissions into tissues. The backing is added to the rear of the transducer in order to damp the acoustic backwave and to reduce the pulse duration. Piezoelectric materials are used to generate and detect ultrasound. In general, broadband transducers should be used for medical ultrasonic imaging. The broad bandwidth response corresponds to a short pulse length, resulting in better axial resolution. Three factors are important in designing broad bandwidth transducers; acoustic impedance matching, a high electromechanical coupling coefficient of the transducer, and electrical impedance matching. These pulse echo transducers operate based on thickness mode resonance of the piezoelectric thin plate. Further, a low planar mode coupling coefficient, k_p, is beneficial for limiting

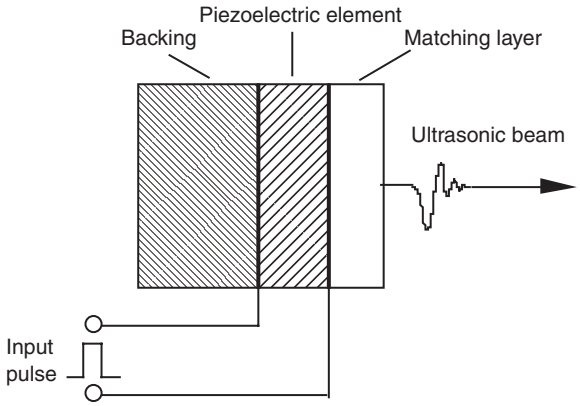

FIGURE 4.1.13 Basic transducer geometry for acoustic imaging applications.

energies being expended in non-productive lateral mode. A large dielectric constant is necessary to enable a good electrical impedance match to the system, especially with tiny piezoelectric sizes.

There are various types of transducers used in ultrasonic imaging. Mechanical sector transducers consist of single, relatively large resonators and can provide images by mechanical scanning such as wobbling. Multiple element array transducers permit discrete elements to be individually accessed by the imaging system and enable electronic focusing in the scanning plane to various adjustable penetration depths through the use of phase delays. Two basic types of array transducers are linear and phased (or sector). A linear array is a collection of elements arranged in one direction, producing a rectangular display (see Figure 4.1.14). A curved linear (or convex) array is a modified linear array whose elements are arranged along an arc to permit an enlarged trapezoidal field of view. The elements of these linear type array transducers are excited sequentially group by group with the sweep of the beam in one direction. These linear array transducers are used for radiological and obstetrical examinations. On the other hand, in a phased array transducer, the acoustic beam is steered by signals that are applied to the elements with delays, creating a sector display. This transducer is useful for cardiology applications where positioning between the ribs is necessary.

4.1.3.5 Resonators/Filters

When a piezoelectric body vibrates at its resonant frequency, it absorbs considerably more energy than at other frequencies resulting in a dramatic decrease

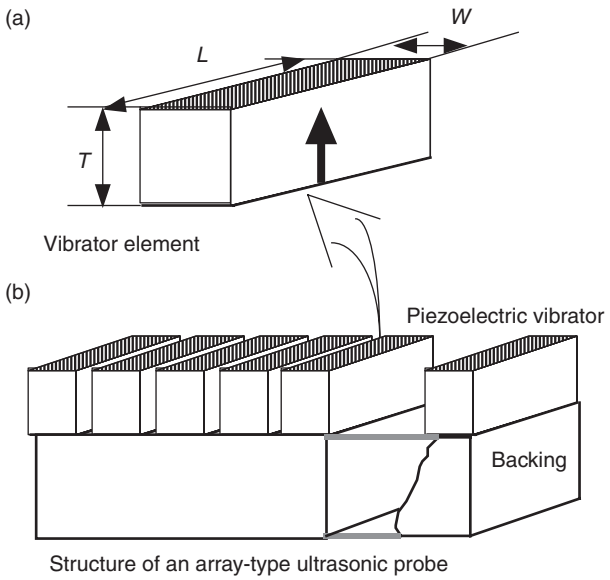

FIGURE 4.1.14 Linear array type ultrasonic probe.

in the impedance. This phenomenon enables piezoelectric materials to be used as a wave filter. A filter is required to pass a certain selected frequency band or to block a given band. The band width of a filter fabricated from a piezoelectric material is determined by the square of the coupling coefficient k, that is, it is nearly proportional to k^2. Quartz crystals with a very low k value of about 0.1 can pass very narrow frequency bands of approximately 1% of the center resonance frequency. On the other hand, PZT ceramics with a planar coupling coefficient of about 0.5 can easily pass a band of 10% of the center resonance frequency. The sharpness of the passband is dependent on the mechanical quality factor Q_M of the materials. Quartz also has a very high Q_M of about 10^6, which results in a sharp cut-off to the passband and a well-defined oscillation frequency.

A simple resonator is a thin disk type, electroded on its plane faces and vibrating radially, for filter applications with a center frequency ranging from 200 kHz to 1 MHz and with a bandwidth of several percent of the center frequency. For a frequency of 455 kHz, the disk diameter needs to be about 5.6 mm. However, if the required frequency is higher than 10 MHz, other modes of vibration such as the thickness extensional mode are exploited, because of its smaller size. The trapped-energy type filters made from PZT ceramics have been widely used in the intermediate frequency range for applications such as the 10.7 MHz FM radio receiver and transmitter. When the trapped-energy phenomena are

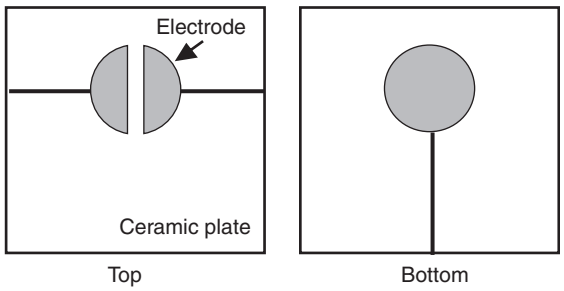

FIGURE 4.1.15 Schematic drawing of a trapped-energy filter.

utilized, the overtone frequencies are suppressed. The plate is partly covered with electrodes of a specific area and thickness. The fundamental frequency of the thickness mode of the ceramic beneath the electrode is less than that of the unelectroded portion, because of the extra inertia of the electrode mass. The lower-frequency wave of the electroded region cannot propagate into the unelectroded region. The higher-frequency overtones, however, can propagate away into the unelectroded region. This is called the *trapped-energy principle*. Figure 4.1.15 shows a schematic drawing of a *trapped-energy filter*. In this structure the top electrode is split so that coupling between the two parts will only be efficient at resonance. More stable filters suitable for telecommunication systems have been made from single crystals such as quartz or $LiTaO_3$.

4.1.4 SURFACE ACOUSTIC WAVE DEVICES

A *surface acoustic wave* (SAW), also called a *Rayleigh wave*, is essentially a coupling between longitudinal and shear waves. The energy carried by the SAW is confined near the surface. An associated electrostatic wave exists for a SAW on a piezoelectric substrate, which allows electroacoustic coupling via a transducer. The advantages of SAW technology are [23, 24]:

1. The wave can be electroacoustically accessed and tapped at the substrate surface and its velocity is approximately 10^4 times slower than an electromagnetic wave.
2. The SAW wavelength is on the same order of magnitude as line dimensions produced by photolithography and the lengths for both short and long delays are achievable on reasonably sized substrates.

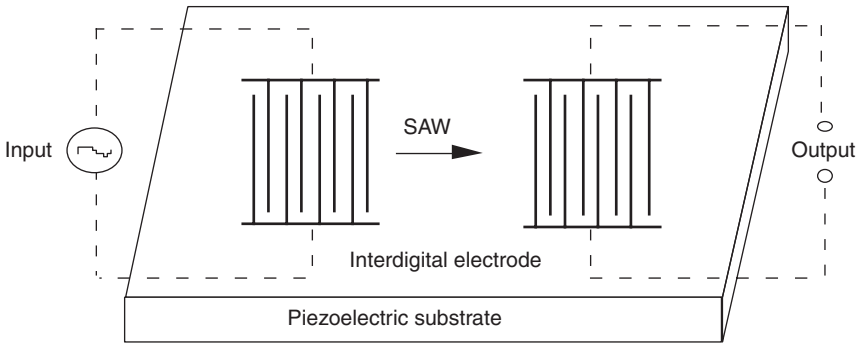

FIGURE 4.1.16 Fundamental structure of a SAW device.

There is a very broad range of commercial system applications which include front-end and intermediate frequency (IF) filters, community antenna television (CATV) and video cassette recorder (VCR) components, synthesizers, analyzers and navigators. In SAW transducers, finger (*interdigital*) electrodes provide the ability to sample or tap the wave and the electrode gap gives the relative delay. A SAW filter is composed of a minimum of two transducers. A schematic of a simple SAW bidirectional filter is shown in Figure 4.1.16. A bidirectional transducer radiates energy equally from each side of the transducer. Energy which is not associated with the received signal is absorbed to eliminate spurious reflection.

Various materials are currently being used for SAW devices. The most popular single-crystal SAW materials are $LiNbO_3$ and $LiTaO_3$. The materials have different properties depending on the cut of the material and the direction of propagation. The fundamental parameters considered when choosing a material for a given device applications are SAW velocity, temperature coefficients of delay (TCD), electromechanical coupling factor and propagation loss. Surface acoustic waves can be generated and detected by spatially periodic, interdigital electrodes on the plane surface of a piezoelectric plate. A periodic electric field is produced when an RF source is connected to the electrode, thus permitting piezoelectric coupling to a traveling surface wave. If an RF source with a frequency, f, is applied to the electrode having periodicity, d, energy conversion from an electrical to mechanical form will be maximum when

$$f = f_0 = v_s/d, \tag{39}$$

where v_s is the SAW velocity and f_0 is the center frequency of the device. The SAW velocity is an important parameter determining the center frequency. Another important parameter for many applications is temperature sensitivity. For example, the temperature stability of the center frequency of SAW bandpass

filters is a direct function of the temperature coefficient for the velocity and the delay for the material used. The first-order temperature coefficient of delay is given by:

$$(1/\tau) \cdot (\mathrm{d}\tau/\mathrm{d}T) = (1/L) \cdot (\mathrm{d}L/\mathrm{d}T)(1/v_s) \cdot (\mathrm{d}v_s/\mathrm{d}T), \tag{40}$$

where $\tau = L/v_s$ is the delay time and L is the SAW propagation length. The surface wave coupling factor, k_s^2, is defined in terms of the change in SAW velocity which occurs when the wave passes across a surface coated with a thin massless conductor, so that the piezoelectric field associated with the wave is effectively short-circuited. The coupling factor, k_s^2, is expressed by:

$$k_s^2 = 2(v_f v_m)/v_f, \tag{41}$$

where v_f is the free surface wave velocity and v_m the velocity on the metallized surface. In actual SAW applications, the value of k_s^2 relates to the maximum bandwidth obtainable and the amount of signal loss between input and output, which determines the fractional bandwidth as a function of minimum insertion loss for a given material and filter. Propagation loss is one of the major factors that determines the insertion loss of a device and is caused by wave scattering at crystalline defects and surface irregularities. Materials which show high electromechanical coupling factors combined with small temperature coefficients of delay are generally preferred. The free surface velocity, v_0, of the material is a function of cut angle and propagation direction. The TCD is an indication of the frequency shift expected for a transducer due to a temperature change and is also a function of cut angle and propagation direction. The substrate is chosen based on the device design specifications which include operating temperature, fractional bandwidth, and insertion loss.

Piezoelectric single crystals such as 128°Y–X (128°-rotated-Y-cut and X-propagation)—$LiNbO_3$ and X–112°Y (X-cut and 112°-rotated-Y-propagation)—$LiTaO_3$ have been extensively employed as SAW substrates for applications in VIF filters. A c-axis oriented ZnO thin film deposited on a fused quartz, glass or sapphire substrate has also been commercialized for SAW devices. Table 4.1.2 summarizes some important material parameters for these SAW materials.

A delay line can be formed from a slice of glass such as PbO or K_2O doped SiO_2 glass in which the velocity of sound is nearly independent of temperature. PZT ceramic transducers are soldered on two metallized edges of the slice of glass. The input transducer converts the electrical signal to a shear acoustic wave which travels through the slice. At the output transducer, the wave is reconverted into an electrical signal delayed by the length of time taken to travel around the slice. Such delay lines are used in color TV sets to introduce a delay of approximately 64 μs and are also employed in videotape recorders.

TABLE 4.1.2 SAW Material Properties

Material	Cut–propagation direction	k^2(%)	TCD (ppm/C)	v_0 (m/s)	ε_r
Single crystal					
Quartz	ST–X	0.16	0	3158	4.5
$LiNbO_3$	128°Y–X	5.5	−74	3960	35
$LiTaO_3$	X112°–Y	0.75	−18	3290	42
$Li_2B_4O_7$	(110)–⟨001⟩	0.8	0	3467	9.5
Ceramic					
PZT–In$(Li_{3/5}W_{2/5})O_3$		1.0	10	2270	690
(Pb, Nd)(Ti, Mn, In)O_3		2.6	<1	2554	225
Thin film					
ZnO/glass		0.64	−15	3150	8.5
ZnO/sapphire		1.0	−30	5000	8.5

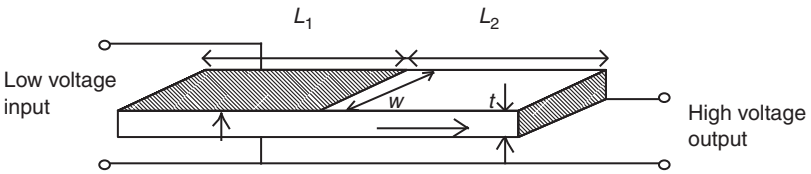

FIGURE 4.1.17 Piezoelectric transformer proposed by Rosen [25].

4.1.5 PIEZOELECTRIC TRANSFORMERS

When input and output terminals are fabricated on a piezo device and input/output voltage is changed through the vibration energy transfer, the device is called a *piezoelectric transformer*. Piezoelectric transformers were used in color TVs because of their compact size in comparison with the conventional electromagnetic coil-type transformers. Since serious problems were found initially in the mechanical strength (collapse occurred at the nodal point!) and in heat generation, the development approach was the same as that used for fabricating ceramic actuators. Recent lap-top computers with a liquid crystal display require a very thin, no electromagnetic-noise transformer to start the glow of a fluorescent back-lamp. This application has recently accelerated the development of the piezotransformer.

Since the original piezotransformer was proposed by Rosen [25], there have been a variety of such transformers investigated. Figure 4.1.17 shows a fundamental structure where two differently poled parts coexist in one piezoelectric plate. A standing wave with a wavelength equal to the sample length is excited,

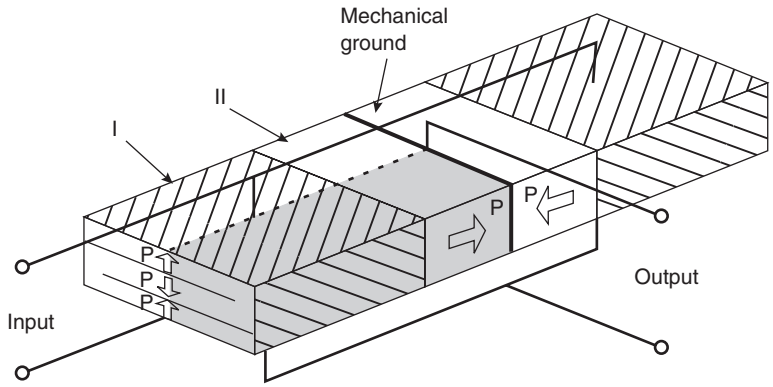

FIGURE 4.1.18 Multilayer type transformer by NEC.

a half wavelength existing on both the input (L_1) and output (L_2) parts. The voltage rise ratio r (*step-up ratio*) is given for the unloaded condition by:

$$r = \left(4/\pi^2\right) k_{31} k_{33} Q_M (L_2/t) \left[2\sqrt{s_{33}^E / s_{11}^E} \Big/ \left(1 + \sqrt{s_{33}^D / s_{11}^E} \right) \right]. \qquad (42)$$

The r ratio is increased with an increase of (L_2/t), where t is the thickness.

NEC proposed a multilayer type transformer (Fig. 4.1.18) in order to increase the voltage rise ratio [26]. Usage of the third-order longitudinal mode is another idea to distribute the stress concentration.

4.1.6 PIEZOELECTRIC ACTUATORS

Piezoelectric and electrostrictive devices have become key components in smart actuator systems such as precision positioners, miniature ultrasonic motors and adaptive mechanical dampers. This section reviews the developments of piezoelectric and related ceramic actuators with particular focus on the improvement of actuator materials, device designs and applications of the actuators.

Piezoelectric actuators are forming a new field between electronic and structural ceramics [27–30]. Application fields are classified into three categories: positioners, motors and vibration suppressors. The manufacturing precision of optical instruments such as lasers and cameras, and the positioning accuracy for fabricating semiconductor chips, which must be adjusted using solid-state actuators, are generally on the order of 0.1 μm. Regarding conventional electromagnetic motors, tiny motors smaller than 1 cm^3 are often required in office

or factory automation equipment and are rather difficult to produce with sufficient energy efficiency. Ultrasonic motors whose efficiency is insensitive to size are considered superior in the mini-motor area. Vibration suppression in space structures and military vehicles using piezoelectric actuators is another promising field of application.

New solid-state displacement transducers controlled by temperature (shape memory alloy) or magnetic field (magnetostrictive alloy) have been proposed, but are generally inferior to the piezoelectric/electrostrictive ceramic actuators because of current technological trends aimed at reduced driving power and miniaturization [30]. The shape memory actuator is too slow in response with a very low energy efficiency, while the magnetostrictor requires a driving coil which is very bulky and generates magnetic noise.

4.1.6.1 Ceramic Actuator Materials

Actuator materials are classified into three categories; piezoelectric, electrostrictive and phase-change materials. Modified lead zirconate titanate [PZT, $Pb(Zr,Ti)O_3$] ceramics are currently the leading materials for piezoelectric applications. The PLZT [$(Pb,La)(Zr,Ti)O_3$] 7/62/38 compound is one such composition [31]. The strain curve is shown in Figure 4.1.19a (left). When the applied field is small, the induced strain x is nearly proportional to the field E ($x = dE$, where d is called the piezoelectric constant). As the field becomes larger (i.e. greater than about 1 kV/cm), however, the strain curve deviates from this linear trend and significant hysteresis is exhibited due to polarization reorientation. This sometimes limits the use of such materials for actuator applications that require non-hysteretic response.

An interesting new family of actuators has been fabricated in Germany from the barium stannate titanate system [$Ba(Sn,Ti)O_3$] [32]. The useful property of $Ba(Sn_{0.15}Ti_{0.85})O_3$ is its unusual strain curve, in which the domain reorientation occurs only at low fields, and there is then a long linear range at higher fields (Figure 4.1.19a, right); that is, the coercive field is unusually small. Moreover, this system is particularly intriguing since it contains no Pb ions, an essential feature as ecological concerns grow in the future.

The second category of actuators is based on electrostriction as exhibited by PMN [$Pb(Mg_{1/3}Nb_{2/3})O_3$] based ceramics. Although it is a second-order phenomenon of electromechanical coupling ($x = ME^2$, where M is called the electrostrictive coefficient), the induced strain can be extraordinarily large (more than 0.1%) [33]. An attractive feature of these materials is the near absence of hysteresis (Fig. 4.1.19b). The superiority of PMN to PZT was demonstrated in a scanning tunneling microscope (STM) [34]. The STM probe was

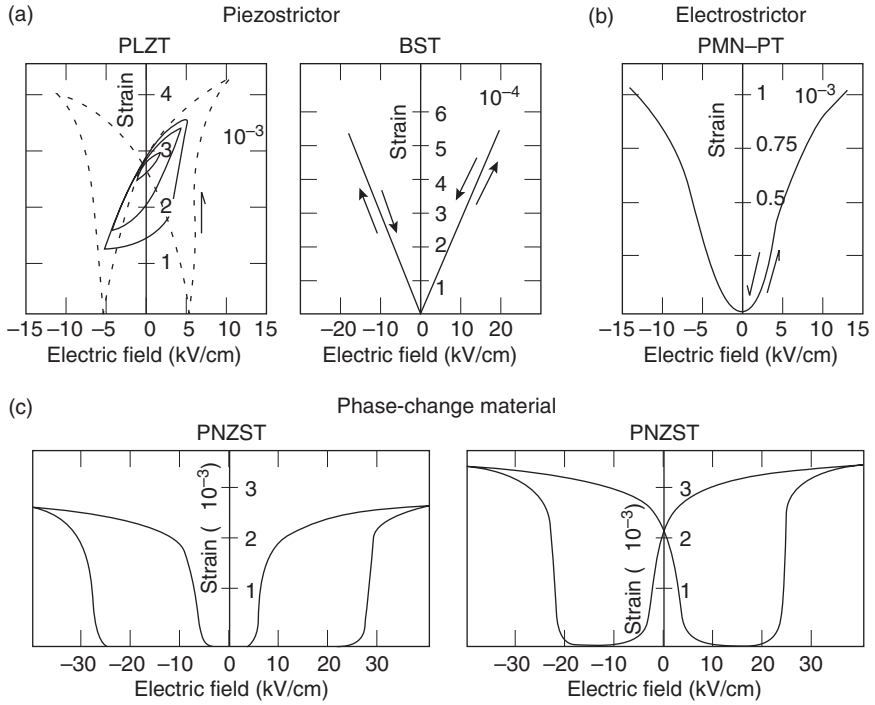

FIGURE 4.1.19 Electric field-induced strains in ceramics: (a) piezoelectric (Pb,La)(Zr,Ti)O_3 and Ba(Sn,Ti)O_3; (b) electrostrictive Pb($Mg_{1/3}Nb_{2/3}$,Ti)O_3; (c) phase-change material Pb(Zr,Sn,Ti)O_3.

scanned mechanically by a PMN actuator, which produces only extremely small distortion of the image, even when the probe was scanned in the opposite direction due to a negligibly small hysteresis.

The third category is based on phase-change-related strains, that is, polarization induced by switching from an antiferroelectric to a ferroelectric state [35]. Figure 4.1.19c shows the field-induced strain curves taken for the lead zirconate stannate based system [$Pb_{0.99}Nb_{0.02}((Zr_xSn_{1-x})_{1-y}Ti_y)_{0.98}O_3$]. The longitudinally induced strain reaches more than 0.3%, which is much larger than that exhibited by normal piezostrictors or electrostrictors. A rectangular-shaped hysteresis in Figure 4.1.19c (left) characterizes the response of these devices which are referred to as "digital displacement transducers" because of the two on/off strain states. Moreover, this field-induced transition is accompanied by a shape memory effect for appropriate compositions (Figure 4.1.19c, right). Once the ferroelectric phase has been induced, the material "memorizes" its ferroelectric state even under zero-field conditions, although it can be

erased with the application of a small reverse bias field [36]. This shape memory ceramic is used in energy saving actuators. A latching relay was composed of a shape memory ceramic unimorph and a mechanical snap action switch, which was driven by a pulse voltage of 4 ms duration. Compared with the conventional electromagnetic relays, the new relay was much simpler and more compact in structure with almost the same response time.

4.1.6.2 Actuator Designs

Two of the most popular actuator designs are the multilayers [37] and bimorphs (see Figure 4.1.20). The multilayer, in which roughly 100 thin piezoelectric/electrostrictive ceramic sheets are stacked together, has the advantages of low driving voltage (100 V), quick response (10 μs), high generative force (1000 N), and high electromechanical coupling. But the displacement, on the order of 10 μm, is not sufficient for some applications. This contrasts with the characteristics of the bimorph which consists of multiple piezoelectric and elastic plates bonded together to generate a large bending displacement of several hundred μm, but has relatively low response time (1 ms) and generative force (1 N).

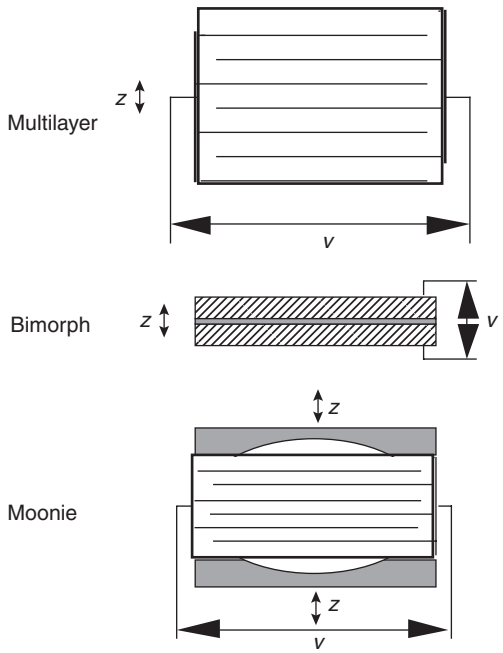

FIGURE 4.1.20 Typical designs for ceramic actuators: multilayer, bimorph and moonie.

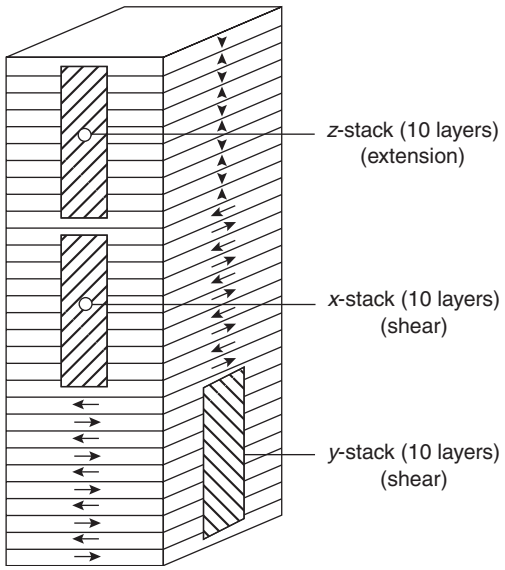

FIGURE 4.1.21 3D positioning multilayer actuator. Notice that the *x*- and *y*-stacks are using shear mode with the spontaneous polarization perpendicular to the applied electric field direction.

A 3D positioning actuator with a stacked structure as pictured in Figure 4.1.21 was proposed by a German company, where shear strain was utilized to generate the *x* and *y* displacements [38]. Polymer-packed PZT bimorphs have been commercialized by ACX for vibration reduction/control applications in smart structures [39].

A composite actuator structure called the "moonie" (or "cymbal") has been developed to provide characteristics intermediate between the multilayer and bimorph actuators; this transducer exhibits an order of magnitude larger displacement than the multilayer, and much larger generative force with quicker response than the bimorph [40]. The device consists of a thin multilayer piezoelectric element and two metal plates with narrow moon-shaped cavities bonded together as shown in Figure 4.1.20. The moonie with a size of $5 \times 5 \times 2.5\,\text{mm}^3$ can generate a $20\,\mu\text{m}$ displacement under 60 V, eight times as large as the generative displacement produced by a multilayer of the same size [41]. This new compact actuator has been utilized in a miniaturized laser beam scanner.

4.1.6.3 Drive/Control Techniques

Piezoelectric/electrostrictive actuators may be classified into two categories, based on the type of driving voltage applied to the device and the nature

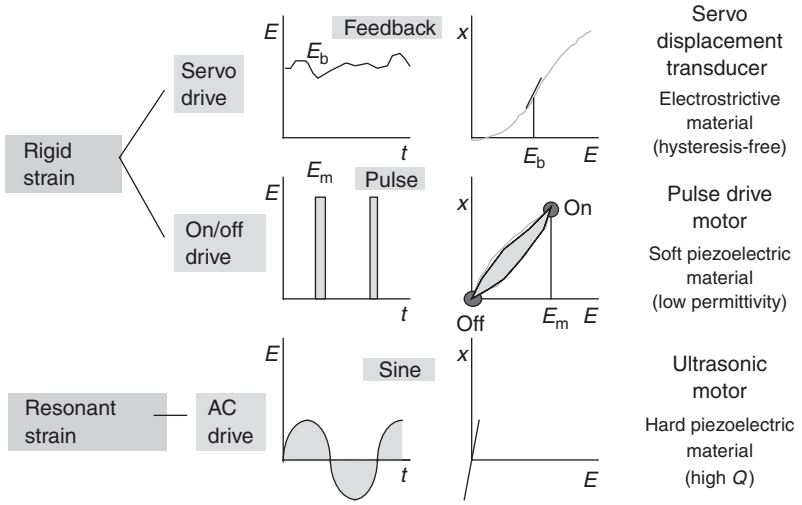

FIGURE 4.1.22 Classification of piezoelectric/electrostrictive actuators.

of the strain induced by the voltage (Fig. 4.1.22): (a) rigid displacement devices for which the strain is induced unidirectionally along the direction of the applied DC field; and (b) resonating displacement devices for which the alternating strain is excited by an AC field at the mechanical resonance frequency (ultrasonic motors). The first can be further divided into two types: servo displacement transducers (positioners) controlled by a feedback system through a position-detection signal, and pulse drive motors operated in a simple on/off switching mode, exemplified by dot-matrix printers.

The material requirements for these classes of devices are somewhat different, and certain compounds will be better suited to particular applications. The ultrasonic motor, for instance, requires a very hard piezoelectric with a high mechanical quality factor Q_M, to suppress heat generation. Driving the motor at the antiresonance frequency, rather than at resonance, is also an intriguing technique to reduce the load on the piezoceramic and the power supply [42]. The servo displacement transducer suffers most from strain hysteresis and, therefore, a PMN electrostrictor is used for this purpose. The pulse drive motor requires a low permittivity material aimed at quick response with a certain power supply rather than a small hysteresis, so soft PZT piezoelectrics are preferred rather than the high-permittivity PMN for this application.

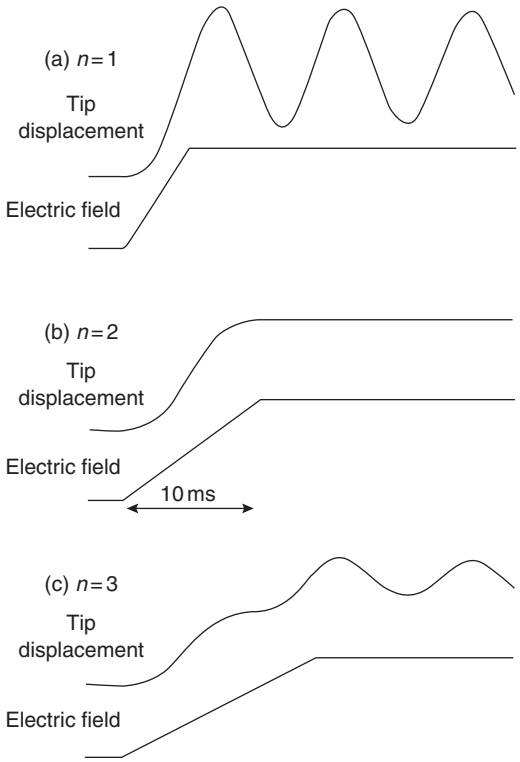

FIGURE 4.1.23 Transient vibration of a bimorph excited after a pseudo-step voltage applied. n is a time scale with a unit of half of the resonance period, that is, $2n$ = resonance period.

Pulse drive techniques for ceramic actuators are very important for improving the response of the device [43, 44]. Figure 4.1.23 shows transient vibrations of a bimorph excited after a pseudo-step voltage is applied. The rise time is varied around the resonance period (n is the time scale with a unit of $T_0/2$, where T_0 stands for the resonance period). It is concluded that the overshoot and ringing of the tip displacement is completely suppressed when the rise time is precisely adjusted to the resonance period of the piezodevice (i.e. for $n = 2$) [43]. A flight actuator was developed using a pulse drive piezoelectric element and a steel ball. A 5 μm rapid displacement induced in a multilayer actuator can hit a 2 mm steel ball up to 20 mm in height. A dot-matrix printer head has been developed using a flight actuator as shown in Figure 4.1.24 [45]. By changing the drive voltage pulse width, the movement of the armature was easily controlled to realize no vibrational ringing or double hitting.

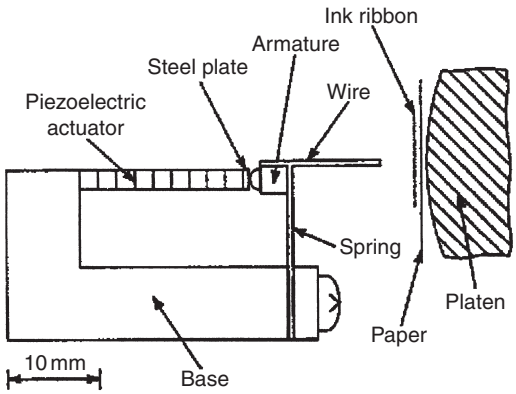

FIGURE 4.1.24 Dot-matrix printer head using a flight actuator mechanism.

4.1.6.4 Device Applications

4.1.6.4.1 Servo Displacement Transducers

A typical example is found in a space truss structure proposed by the Jet Propulsion Laboratory [46]. A stacked PMN actuator was installed at each truss nodal point and operated so that unnecessary mechanical vibration was suppressed immediately. A "Hubble" telescope has also been proposed using multilayer PMN electrostrictive actuators to control the phase of the incident light wave in the field of optical information processing (Fig. 4.1.25) [47]. The PMN electrostrictor provided superior adjustment of the telescope image because of negligible strain hysteresis.

The US Army is interested in developing a rotor control system in helicopters. Figure 4.1.26 shows a bearingless rotor flexbeam with attached piezoelectric strips [48]. Various types of PZT-sandwiched beam structures have been investigated for such a flexbeam application and for active vibration control [49].

Concerning home appliance applications, there is already a large market in VCR systems. The requirement for high-quality images has become very stringent for VCRs especially when played in still, slow or quick mode. As illustrated in Figure 4.1.27, when the tape is running at a speed different from the normal speed, the head trace deviates from the recording track depending on the velocity difference. Thus, the head traces on the guard band, generating *guard band noise* [50]. The auto tracking scan system by Ampex operates with a piezoelectric actuator so that the head follows the recording track. The piezoelectric device generates no magnetic noise.

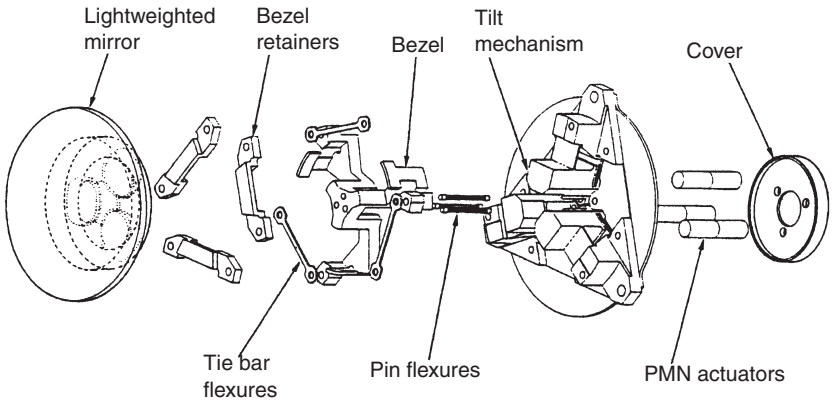

FIGURE 4.1.25 "Hubble" telescope using three PMN electrostrictive actuators for optical image correction.

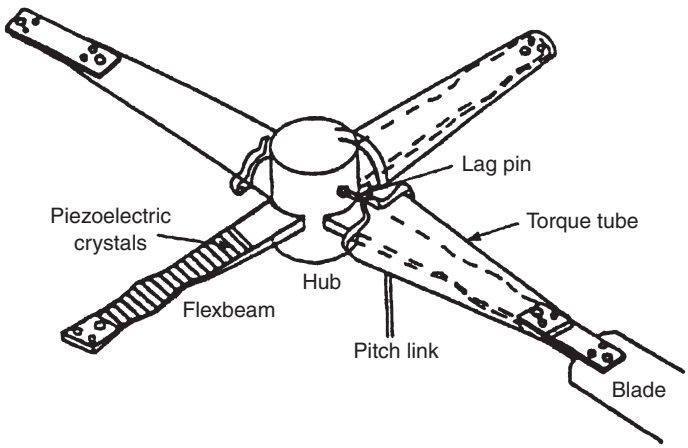

FIGURE 4.1.26 Bearingless rotor flexbeam with attached piezoelectric strips. A slight change in the blade angle provides for enhanced controllability.

Bimorph structures are commonly used for this tracking actuator because of their large displacement. However, special care has been taken not to produce a *spacing angle* between the head and the tape, because a single bimorph exhibits deflection with slight rotation. Various designs have been proposed to produce a completely parallel motion.

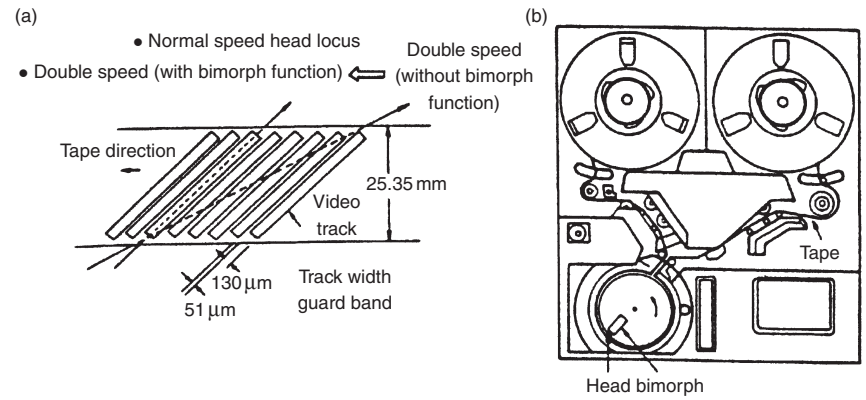

FIGURE 4.1.27 Locus of the video head and the function of the piezoactuator.

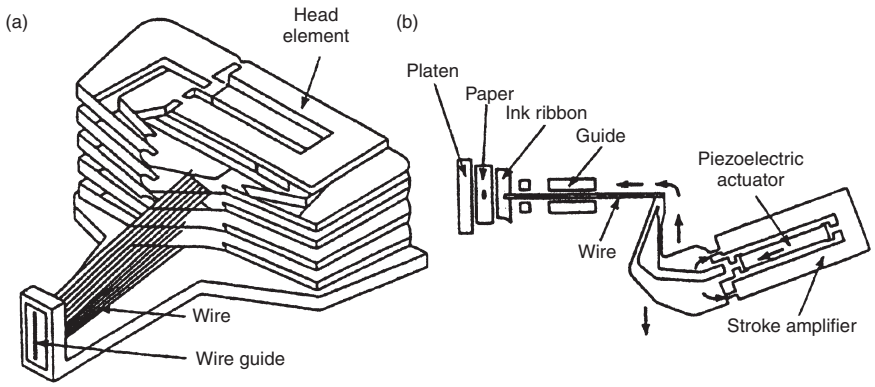

FIGURE 4.1.28 Structure of a printer head (a), and a differential-type piezoelectric printer-head element (b). A sophisticated monolithic hinge lever mechanism amplifies the actuator displacement by 30 times.

4.1.6.4.2 Pulse Drive Motors

A dot-matrix printer is the first widely commercialized product using ceramic actuators. Each character formed by such a printer is composed of a 24×24 dot matrix. A printing ribbon is subsequently impacted by a multiwire array. A sketch of the printer head appears in Figure 4.1.28a [51]. The printing element is composed of a multilayer piezoelectric device, in which 100 thin ceramic sheets 100 μm in thickness are stacked, together with a sophisticated magnification mechanism (Fig. 4.1.28b). The magnification unit is based on a monolithic

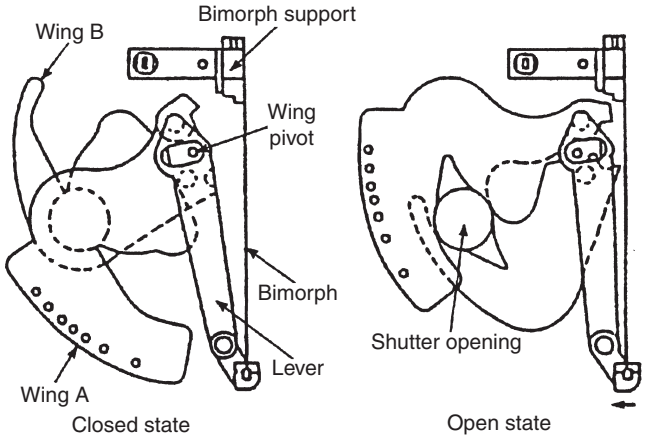

FIGURE 4.1.29 Camera shutter mechanism using a piezoelectric bimorph actuator.

hinge lever with a magnification of 30, resulting in an amplified displacement of 0.5 mm and an energy transfer efficiency greater than 50%.

A piezoelectric camera shutter is currently the largest production item (Fig. 4.1.29). A piece of piezoelectric bimorph can open and close the shutter in a milli-second through a mechanical wing mechanism [52].

Toyota developed a Piezo TEMS (Toyota Electronic Modulated Suspension), which is responsive to each protrusion on the road in adjusting the damping condition, and installed it on a "Celcio" (equivalent to Lexus, internationally) in 1989 [53]. In general, as the damping force of a shock absorber in an automobile is increased (i.e. "hard" damper), the controllability and stability of a vehicle are improved. However, comfort is sacrificed because the road roughness is easily transferred to the passengers. The purpose of the electronically controlled shock absorber is to obtain both controllability and comfort simultaneously. Usually the system is set to provide a low damping force ("soft") so as to improve comfort, and the damping force is changed to a high position according to the road condition and the car speed to improve the controllability. In order to respond to a road protrusion, a very high response of the sensor and actuator combination is required.

Figure 4.1.30 shows the structure of the electronically controlled shock absorber. The sensor is composed of five layers of 0.5 mm thick PZT disks. The detecting speed of the road roughness is about 2 ms and the resolution of the up–down deviation is 2 mm. The actuator is made of 88 layers of 0.5 mm thick disks. Applying 500 V generates a displacement of about 50 μm, which is magnified by 40 times through a piston and plunger pin combination. This

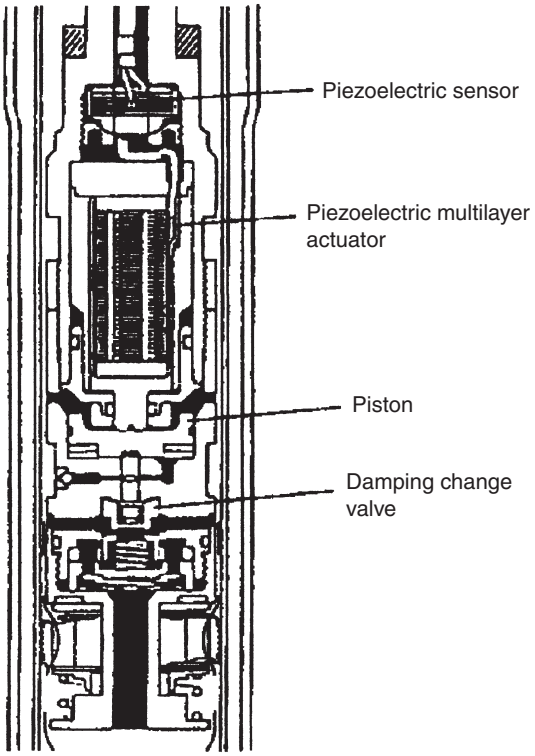

FIGURE 4.1.30 Electronic modulated suspension by Toyota.

stroke pushes the change valve of the damping force down, then opens the bypass oil route, leading to the decrease of the flow resistance (i.e. "soft").

Figure 4.1.31 illustrates the operation of the suspension system. The up–down acceleration and pitching rate were monitored when the vehicle was driven on a rough road. When the TEMS system was used (top figure), the up–down acceleration was suppressed to as small as the condition fixed at "soft", providing comfort. At the same time, the pitching rate was also suppressed to as small as the condition fixed at "hard", leading to better controllability.

Figure 4.1.32 shows a walking piezomotor with four multilayer actuators [54]. The two shorter actuators function as clamps and the longer two provide the movement by an inchworm mechanism.

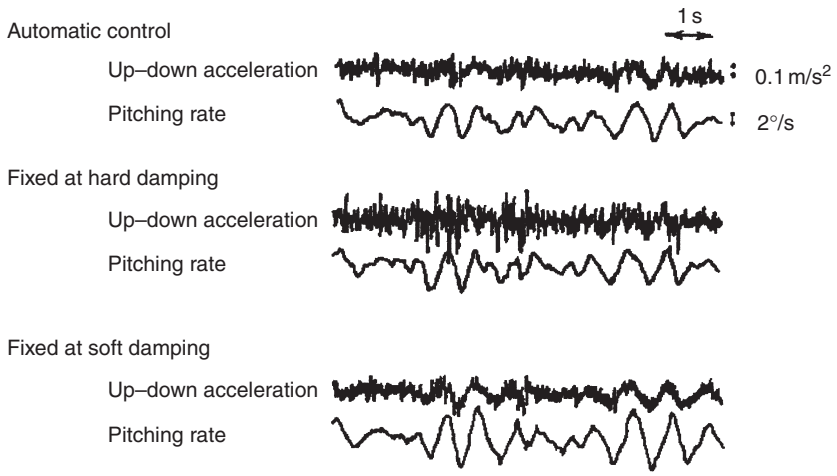

FIGURE 4.1.31 Function of the adaptive suspension system.

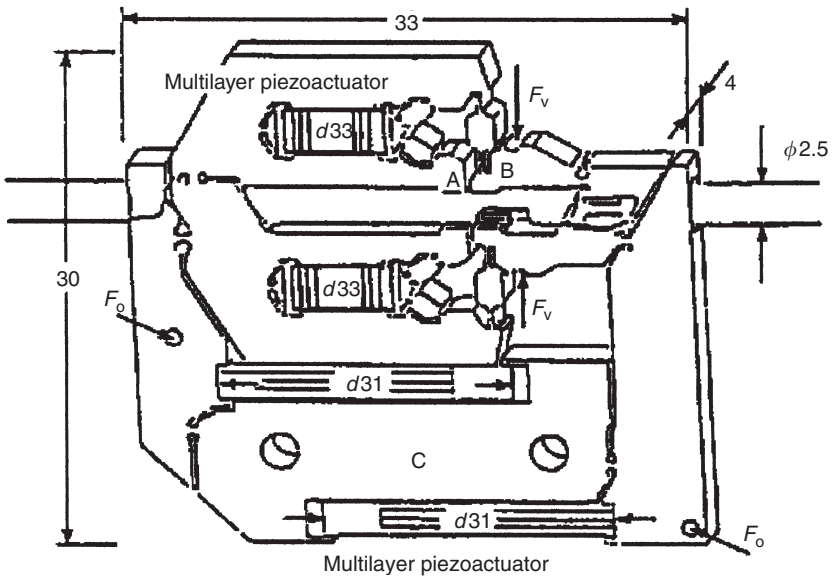

FIGURE 4.1.32 Walking piezomotor using an inchworm mechanism with four multilayer piezoelectric actuators by Philips.

4.1.6.4.3 Ultrasonic Motors

4.1.6.4.3.1 *Background*

Electromagnetic motors were invented more than a 100 years ago. While these motors still dominate the industry, a drastic improvement cannot be expected except through new discoveries in magnetic or superconducting materials. Regarding conventional electromagnetic motors, tiny motors smaller than 1 cm^3 are rather difficult to produce with sufficient energy efficiency. Therefore, a new class of motors using high power ultrasonic energy, the ultrasonic motor, is gaining widespread attention. Ultrasonic motors made with piezoceramics whose efficiency is insensitive to size are superior in the mini-motor area. Figure 4.1.33 shows the basic construction of most ultrasonic motors, which consist of a high-frequency power supply, a vibrator and a slider. The vibrator is composed of a piezoelectric driving component and an elastic vibratory part, and the slider is composed of an elastic moving part and a friction coat.

Although there had been some earlier attempts, the first practical ultrasonic motor was proposed by H. V. Barth of IBM in 1973 [55]. The rotor was pressed against two horns placed at different locations. By exciting one of the horns, the rotor was driven in one direction, and by exciting the other horn, the rotation direction was reversed. Various mechanisms based on virtually the same principle were proposed by Lavrinenko [56] and Vasiliev [57] in the former USSR. Because of difficulty in maintaining a constant vibration amplitude with temperature rise, wear and tear, the motors were not of much practical use at that time.

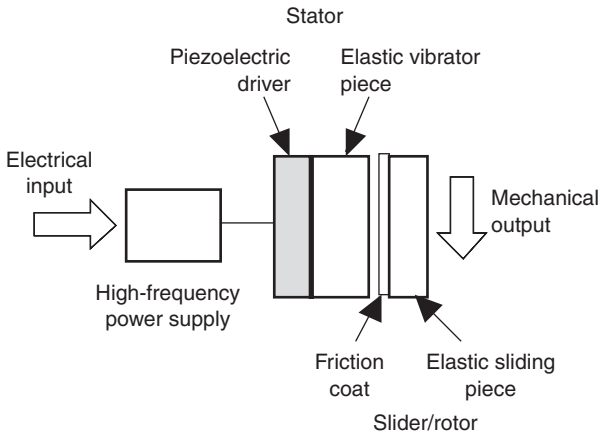

FIGURE 4.1.33 Fundamental construction of an ultrasonic motor.

In the 1980s, with increasing chip pattern density, the semiconductor industry began to demand much more precise and sophisticated positioners which would not generate magnetic field noise. This urgent need accelerated the development of ultrasonic motors. Another advantage of ultrasonic motors over conventional electromagnetic motors with expensive copper coils is the improved availability of piezoelectric ceramics at reasonable cost. Japanese manufacturers are currently producing piezoelectric buzzers at about 30–40 cents per unit.

Let us summarize the merits and demerits of the ultrasonic motor:

Merits

1. Low speed and high torque
   direct drive
2. Quick response, wide velocity range, hard brake and no backlash
   excellent controllability
   fine position resolution
3. High power/weight ratio and high efficiency
4. Quiet drive
5. Compact size and light weight
6. Simple structure and easy production process
7. Negligible effect from external magnetic or radioactive fields, and also no generation of these fields.

Demerits

8. Necessity for a high-frequency power supply
9. Less durability due to frictional drive
10. Drooping torque versus speed characteristics

4.1.6.4.3.2 *Classification and principles of ultrasonic motors*

From a customer's point of view, there are rotary and linear type motors. If we categorize them according to the vibrator shape, there are rod type, π-shaped, ring (square) and cylinder types. Two categories are being investigated for ultrasonic motors from a vibration characteristic viewpoint: a standing-wave type and a propagating-wave type. Refresh your memory on the wave formulas. The standing wave is expressed by

$$u_s(x,t) = A\cos kx \cdot \cos\ \omega t, \tag{43}$$

while the propagating wave is expressed as

$$u_p(x,t) = A\cos(kx - \omega t). \tag{44}$$

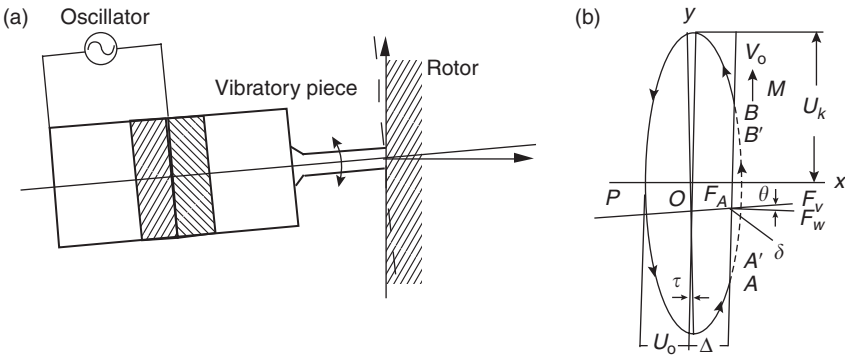

FIGURE 4.1.34 Vibratory coupler type motor (a) and its tip locus (b).

Using a trigonometric relation, Eq. 44 can be transformed as

$$u_p(x,t) = A\cos kx \cdot \cos\,\omega t + A\cos(kx - \pi/2) \cdot \cos(\omega t - \pi/2). \qquad (45)$$

This leads to an important result, a propagating wave can be generated by superimposing two standing waves whose phases differ by 90° both in time and in space. This principle is necessary to generate a propagating wave on a limited volume/size substance, because only standing waves can be excited stably in a solid medium of finite size.

The standing-wave type is sometimes referred to as a vibratory-coupler type or a "woodpecker" type, where a vibratory piece is connected to a piezoelectric driver and the tip portion generates a flat-elliptical movement. Figure 4.1.34 shows a simple model proposed by Sashida [58]. A vibratory piece is attached to a rotor or a slider with a slight cant angle. When a vibration is excited at the piezoelectric vibrator, the vibratory piece generates bending because of restriction by the rotor, so that the tip moves along the rotor face between A → B, and freely between B → A. If the vibratory piece and the piezovibrator are tuned properly, they form a resonating structure, which is an elliptical locus. Therefore, only the duration A → B provides a unidirectional force to the rotor through friction, and, therefore, an intermittent rotational torque or thrust. However, because of the inertia of the rotor, the rotation speed ripple is not observed to be large. The standing-wave type, in general, is low in cost (one vibration source) and has high efficiency (up to 98% theoretically), but lacks control in both the clockwise and counterclockwise directions.

By comparison, the propagating-wave type (a surface-wave or "surfing") combines two standing waves with a 90° phase difference both in time and in space. The principle is shown in Figure 4.1.35. A surface particle of the elastic body draws an elliptical locus due to the coupling of longitudinal and transverse

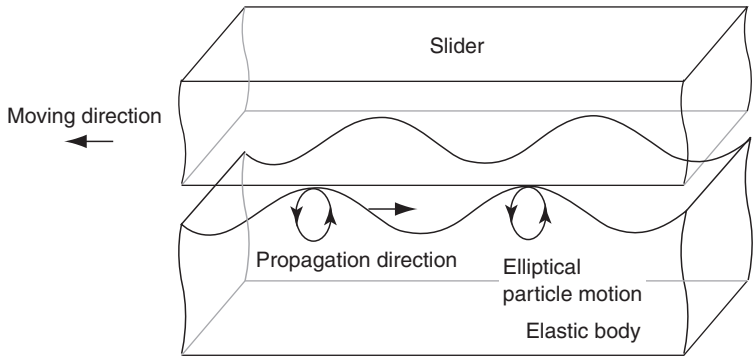

FIGURE 4.1.35 Principle of the propagating-wave type motor.

waves. This type requires, in general, two vibration sources to generate one propagating wave, leading to low efficiency (not more than 50%), but it is controllable in both rotational directions.

4.1.6.4.3.3 *Various ultrasonic motors*

Sashida developed a rotary-type motor similar to the fundamental structure [58]. Four vibratory pieces were installed on the edge face of a cylindrical vibrator, and pressed onto the rotor. This is one of the prototypes which triggered the present active development of ultrasonic motors. A rotation speed of 1500 rpm, torque of 0.08 N m and an output of 12 W (efficiency 40%) are obtained under an input of 30 W at 35 kHz. This type of ultrasonic motor can provide a speed much higher than the inchworm types, because of its high operating frequency and amplified vibration displacement at the resonance frequency.

Hitachi Maxel significantly improved the torque and efficiency by using a torsional coupler replacing Sashida's vibratory pieces (Fig. 4.1.36), and by increasing the pressing force with a bolt [59]. The torsional coupler looks like an old-fashioned TV channel knob, consisting of two legs which transform longitudinal vibration generated by the Langevin vibrator to a bending mode of the knob disk, and a vibratory extruder. Notice that this extruder is aligned with a certain cant angle to the legs, which transforms the bending to a torsional vibration. This transverse moment coupled with the bending up–down motion leads to an elliptical rotation on the tip portion, as illustrated in Figure 4.1.36b. The optimum pressing force to get the maximum thrust is obtained, when the ellipse locus is deformed roughly by half. A motor 30 mm × 60 mm in size and with a 20–30° in cant angle between leg and vibratory piece can generate torques as high as 1.3 N m with an efficiency of 80%. However, this type provides only unidirectional rotation. Notice that even though the drive of the

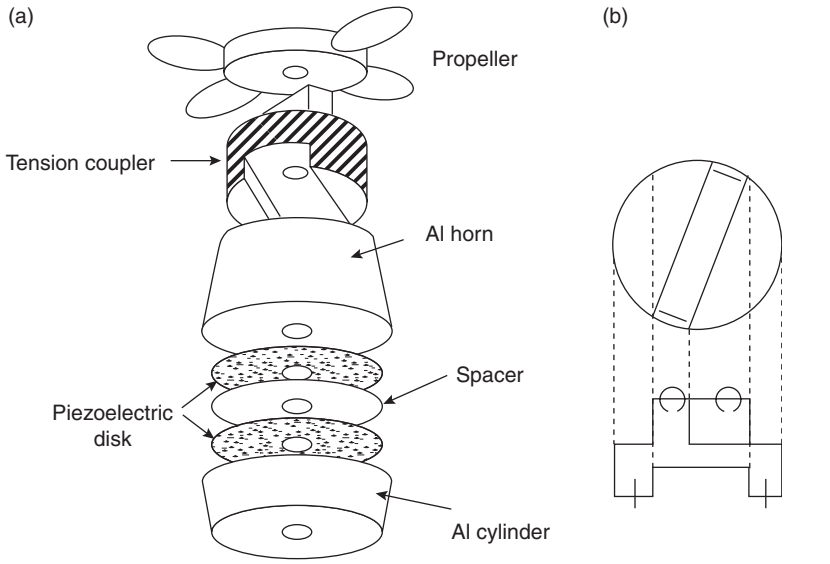

FIGURE 4.1.36 Torsional coupler ultrasonic motor (a) and the motion of the torsional coupler (b).

motor is intermittent, the output rotation becomes very smooth because of the inertia of the rotor.

A compact ultrasonic rotory motor, as tiny as 3 mm in diameter, has been developed at the Pennsylvania State University. As shown in Figure 4.1.37, the stator consists of a piezoelectric ring and two concave/convex metal endcaps with "windmill" shaped slots bonded together, so as to generate a coupling of the up–down and torsional vibrations [60]. Since the number of components is reduced and the fabrication process is much simplified, the fabrication price is decreased remarkably, and a disposable design becomes feasible. When driven at 160 kHz, a maximum revolution of 600 rpm and a maximum torque of 1 mN m were obtained for a 11 mm diameter motor.

Tokin developed a piezoelectric ceramic cylinder for a torsional vibrator [61]. Using an interdigital type electrode pattern printed with a 45° cant angle on the cylinder surface, torsion vibration was generated, which is applicable for a simple ultrasonic motor.

Ueha proposed a two-vibration-mode coupled type (Fig. 4.1.38), that is, a torsional Langevin vibrator was combined with three multilayer actuators to generate larger longitudinal and transverse surface displacements of the stator, as well as to control their phase difference [62]. The phase change can change the rotation direction.

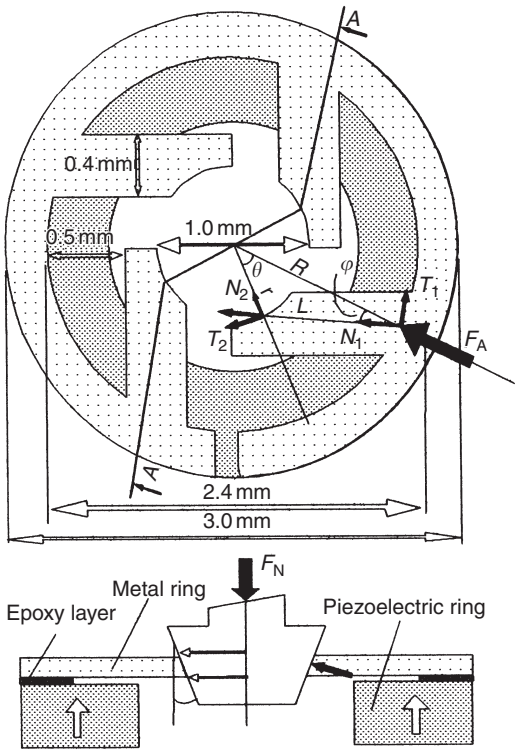

FIGURE 4.1.37 "Windmill" motor with a disk-shaped torsional coupler.

Uchino invented a π-shaped linear motor [63]. This linear motor is equipped with a multilayer piezoelectric actuator and fork-shaped metallic legs as shown in Figure 4.1.39. Since there is a slight difference in the mechanical resonance frequency between the two legs, the phase difference between the bending vibrations of both legs can be controlled by changing the drive frequency. The walking slider moves in a way similar to a horse using its fore and hind legs when trotting. A test motor, $20 \times 20 \times 5\ \text{mm}^3$ in dimension, exhibits a maximum speed of 20 cm/s and a maximum thrust of 0.2 kgf with a maximum efficiency of 20%, when driven at 98 kHz at 6 V (actual power = 0.7 W). This motor has been employed in a precision *X*–*Y* stage.

Tomikawa's rectangular plate motor is also intriguing [64]. As shown in Figure 4.1.40, a combination of the two modes of vibration forms an elliptical displacement. The two modes chosen were the first longitudinal mode (L_1 mode) and the eighth bending mode (B_8), whose resonance frequencies were almost the same. By applying voltages with a phase difference of 90° to

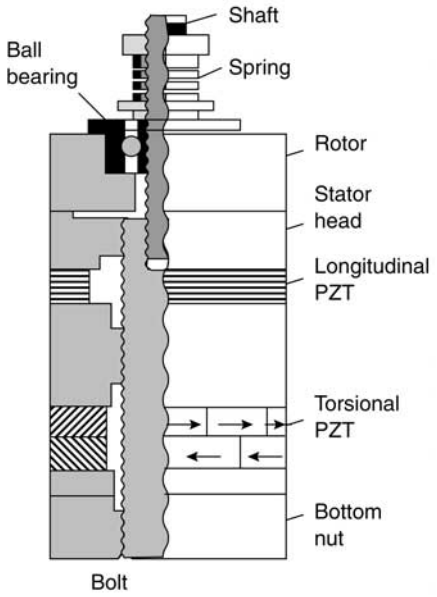

FIGURE 4.1.38 Two-vibration-mode coupled type motor.

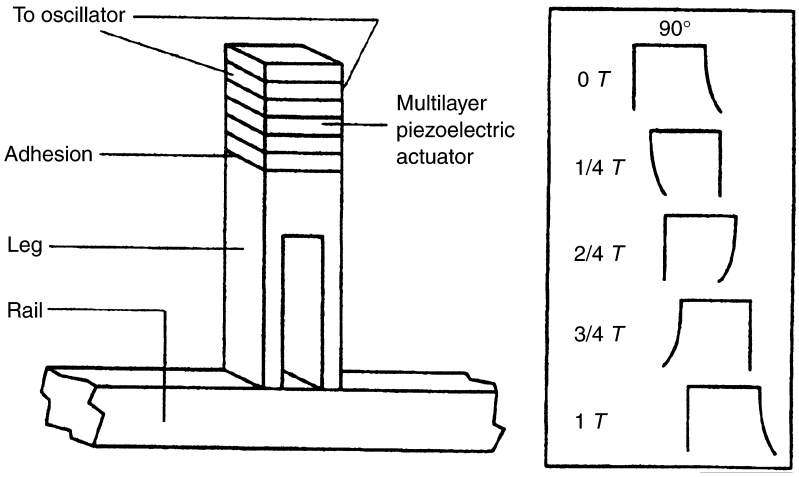

FIGURE 4.1.39 π-shaped linear ultrasonic motor: (a) construction and (b) walking principle. Note the 90° phase difference of two legs similar to that associated with human walking.

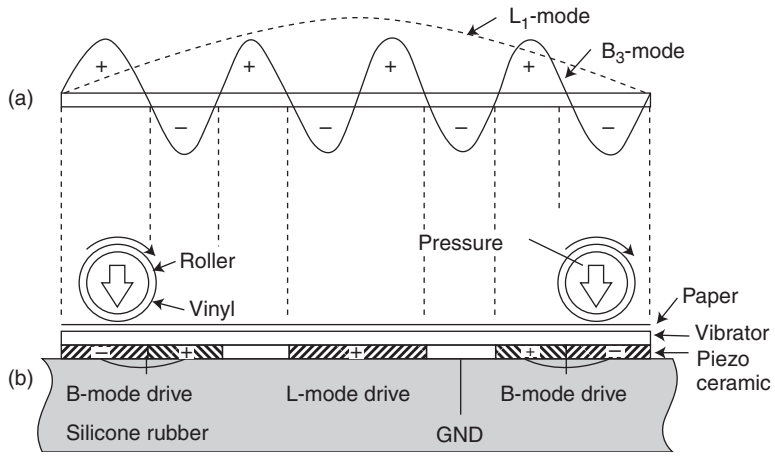

FIGURE 4.1.40 L_1 and B_8 double-mode vibrator motor.

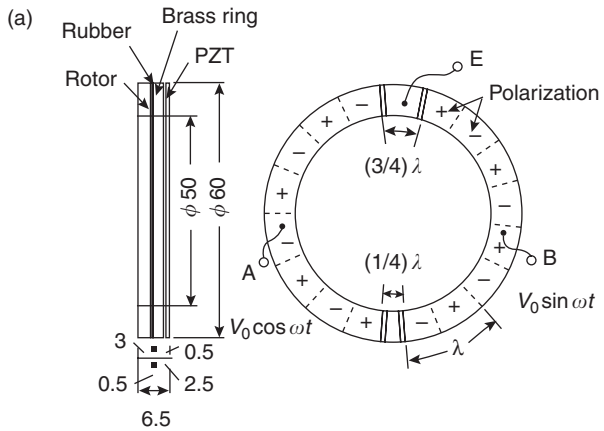

FIGURE 4.1.41 Stator structure of Sashida's motor.

the L- and B-mode drive electrodes, elliptical motion in the same direction can be obtained at both ends of this plate, leading to rotation of the rollers in contact with these points. Anticipated applications are paper or card senders.

Figure 4.1.41 shows the famous Sashida motor [65]. By means of the traveling elastic wave induced by a thin piezoelectric ring, a ring-type slider in contact with the "rippled" surface of the elastic body bonded onto the piezoelectric is driven in both directions by exchanging the sine and cosine voltage inputs. Another advantage is its thin design, which makes it suitable for installation in

cameras as an automatic focusing device. Eighty percent of the exchange lenses in Canon's "EOS" camera series have already been replaced by the ultrasonic motor mechanism.

The PZT piezoelectric ring is divided into 16 positively and negatively poled regions and two asymmetric electrode gap regions so as to generate a ninth mode propagating wave at 44 kHz. A prototype was composed of a brass ring of 60 mm in outer diameter, 45 mm in inner diameter and 2.5 mm in thickness, bonded onto a PZT ceramic ring of 0.5 mm in thickness with divided electrodes on the back-side. The rotor was made of polymer coated with hard rubber or polyurethane. Figure 4.1.42 shows Sashida's motor characteristics.

Canon utilized the "surfing" motor for a camera automatic focusing mechanism, installing the ring motor compactly in the lens frame. It is noteworthy that the stator elastic ring has many teeth, which can magnify the transverse elliptical displacement and improve the speed. The lens position can be shifted back and forth with a screw mechanism. The advantages of this motor over the conventional electromagnetic motor are:

1. Silent drive due to the ultrasonic frequency drive and no gear mechanism (i.e. more suitable for video cameras with microphones).
2. Thin motor design and no speed reduction mechanism such as gears, leading to space saving.
3. Energy saving.

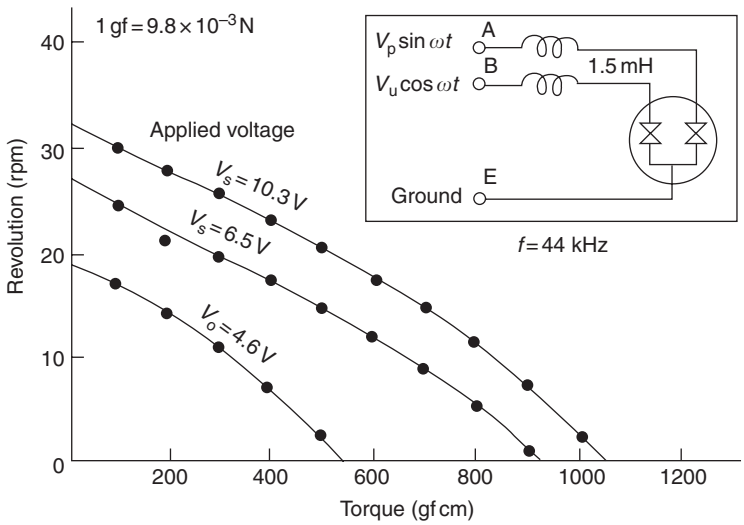

FIGURE 4.1.42 Motor characteristics of Sashida's motor.

A general problem encountered for these traveling-wave type motors is the support of the stator. In the case of a standing-wave motor, the nodal points or lines are generally supported; this causes minimum effects on the resonance vibration. A traveling wave, however, does not have such steady nodal points or lines. Thus, special considerations are necessary. In Figure 4.1.41, the stator is basically supported very gently along the axial direction on felt so as not to suppress the bending vibration. It is important to note that the stop pins which latch onto the stator teeth only provide high rigidity against the rotation.

Matsushita Electric proposed a nodal line support method using a higher-order vibration mode [66]. A stator wide ring is supported at the nodal circular line and "teeth" are arranged on the maximum amplitude circle to get larger revolution.

Seiko Instruments miniaturized the ultrasonic motor to dimensions as tiny as 10 mm in diameter using basically the same principle [67]. Figure 4.1.43 shows the construction of one of these small motors with a 10 mm diameter and a 4.5 mm thickness. A driving voltage of 3 V and a current of 60 mA produces 6000 rpm (no-load) with a torque of 0.1 mN m. Allied Signal developed ultrasonic motors similar to Shinsei's, which are utilized as mechanical switches for launching missiles [68].

It is important to note that the unimorph (a piezoceramic plate and a metal plate bonded together) bending actuation cannot provide high efficiency theoretically, because the electromechanical coupling factor k is usually less than 10%. Therefore, instead of the unimorph structure, a simple disk was

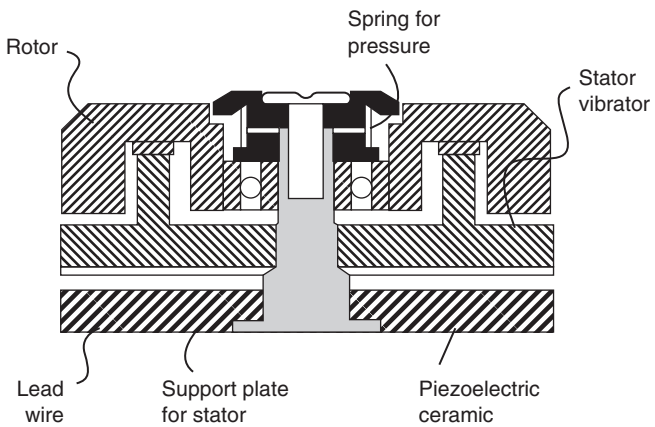

FIGURE 4.1.43 Construction of Seiko's motor.

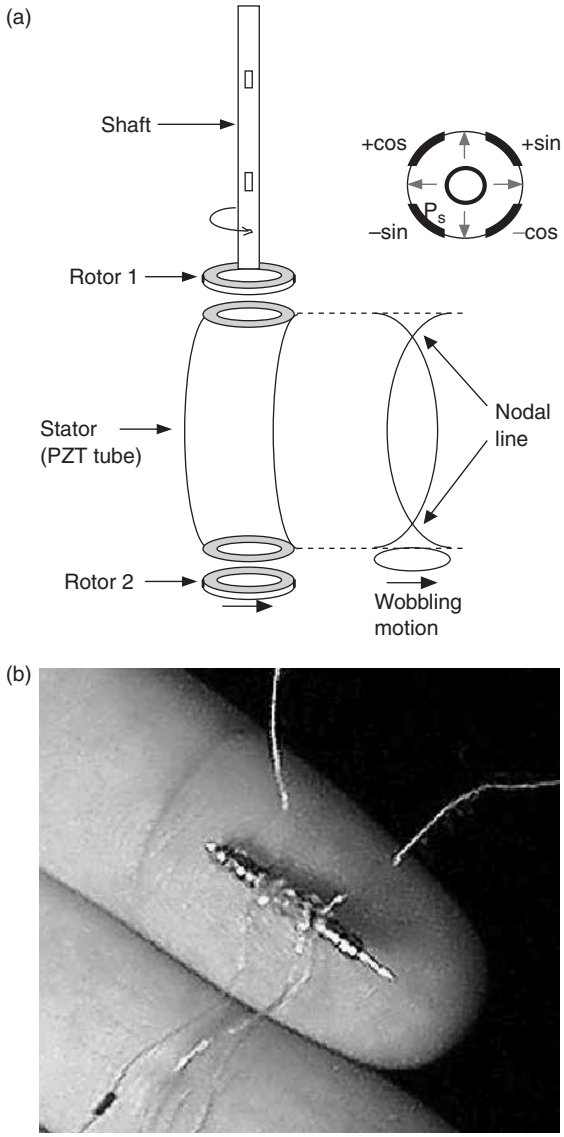

FIGURE 4.1.44 "Plate-spinning" type motor by Penn State and IMRE (1.5 mm in diameter).

directly used to make motors [69, 70]. The (1,1), (2,1) and (3,1) modes of a simple disk, which are axial-asymmetric modes, are proposed to use. Both the inner and outer circumferences can provide a rotation like a "hula hoop."

Another intriguing design is a "plate-spinning" type proposed by Tokin [71]. Penn State and IMRE miniaturized the size down to 1.5 mm in diameter [72]. Figure 4.1.44 shows its principle of operation and a photograph. A rotary bending vibration is excited on a PZT rod by a combination of sine and cosine voltages, then to rotors are brought into contact with the "spinning" rod at the end faces to produce the rotation.

In summary, the standing-wave type, in general, is low in cost (one vibration source) and has high efficiency (up to 98% theoretically), but lack of control in both the clockwise and counterclockwise directions is a problem. In comparison, the propagating-wave type combines two standing waves with a 90° phase difference both in time and space. This type requires, in general, two vibration sources to generate one propagating wave, leading to low efficiency (not more than 50%), but it is controllable in both rotational directions.

REFERENCES

1. Jaffe, B., Cook, W., and Jaffe, H. (1971). *Piezoelectric Ceramics*, London: Academic Press.
2. Cady, W. G. (1964). *Piezoelectricity*, New York: McGraw-Hill, Revised Edition by Dover Publications.
3. Lines, M. E., and Glass, A. M. (1977). *Principles and Applications of Ferroelectric Materials*, Oxford: Clarendon Press.
4. Uchino, K. (1996). *Piezoelectric Actuators and Ultrasonic Motors*, Boston, MA: Kluwer Academic Publishers.
5. Uchino, K. (1986). *Piezoelectric/Electrostrictive Actuators*, Tokyo: Morikita Publishing.
6. Ikeda, T. (1984). *Fundamentals of Piezoelectric Materials Science*, Tokyo: Ohm Publishing Co.
7. Ito, Y., and Uchino, K. (1999). Piezoelectricity, *Wiley Encyclopedia of Electrical and Electronics Engineering*, Vol. 16, p. 479, New York: John Wiley & Sons.
8. Smith, W. A. (1992). *Proc. SPIE—The International Society for Optical Engineering*, 1733.
9. Takeuchi, H., Jyomura, S., Yamamoto, E., and Ito, Y. (1982). *J. Acoust. Soc. Am.* **74**: 1114.
10. Yamashita, Y., Yokoyama, K., Honda, H., and Takahashi, T. (1981). *Jpn. J. Appl. Phys.* **20**: 183.
11. Ito, Y., Takeuchi, H., Jyomura, S., Nagatsuma, K., and Ashida, S. (1979). *Appl. Phys. Lett.* **35**: 595.
12. Takeuchi, H., Masuzawa, H., Nakaya, C., and Ito, Y. (1990). "Proc. IEEE 1990 Ultrasonics Symposium", p. 697.
13. Kuwata, J., Uchino, K., and Nomura, S. (1982). *Jpn. J. Appl. Phys.* **21**: 1298.
14. Shrout, T. R., Chang, Z. P., Kim, N., and Markgraf, S. (1990). *Ferroelectric Lett.* **12**: 63.
15. Newnham, R. E., Skinner, D. P., and Cross, L. E. (1978). *Mater. Res. Bull.* **13**: 525.
16. Smith, W. A. (1989). "Proc. 1989 IEEE Ultrasonic Symposium", p. 755.
17. Kistler, Stress Sensor, Production Catalog, Switzerland.
18. Tokin, Gyroscope, Production Catalog, Japan.
19. Uchino, K., Nomura, S., Cross, L. E., Jang, S. J., and Newham, R. E. (1981). *Jpn. J. Appl. Phys.* **20**: L367. Uchino, K. Proc. Study Committee on Barium Titanate, XXXI-171-1067 (1983).
20. Auld, B. A. (1990). *Acoustic Fields and Waves in Solids*, 2nd edn, Melbourne: Robert E. Krieger.
21. Kino, G. S. (1987). *Acoustic Waves: Device Imaging and Analog Signal Processing*, Englewood Cliffs, NJ: Prentice-Hall.

22. Desilets, C. S., Fraser, J. D., and Kino, G. S. (1978). *IEEE Trans. Sonics Ultrason.* **SU-25**: 115.
23. Campbell, C. (1989). *Surface Acoustic Wave Devices and Their Signal Processing Applications*, San Diego, CA: Academic Press.
24. Matthews, H. (1977). *Surface Wave Filters*, New York: Wiley Interscience.
25. Rosen, C. A. (1957). "Proc. Electronic Component Symp.", p. 205.
26. Kawashima, S., Ohnishi, O., Hakamata, H., Tagami, S., Fukuoka, A., Inoue, T., and Hirose, S. (1994). "Proc. IEEE Int'l Ustrasonic Symp. '94", France.
27. Uchino, K. (1986). *Bull. Am. Ceram. Soc.* **65**: 647.
28. Uchino, K. (1993). *MRS Bull.* **18**: 42.
29. Uchino, K., Editor in Chief (1994). *Handbook on New Actuators for Precision Position Control*, Tokyo: Fuji Technosystem.
30. Uchino, K. (1996). Recent developments in ceramic actuators, "Proc. Workshop on Microsystem Technologies in the USA and Canada, Germany, mst news, special issue, VDI/VDE", pp. 28–36.
31. Furuta, K., and Uchino, K. (1986). *Adv. Ceram. Mater.* **1**: 61.
32. von Cieminski, J., and Beige, H. (1991). *J. Phys. D* **24**: 1182.
33. Cross, L. E., Ang, S. J. J., Newnham, R. E., Nomura, S., and Uchino, K. (1980). *Ferroelectrics* **23**: 187.
34. Uchino, K. (1988). Ceramic actuators, *Ceramic Data Book '88*, Tokyo: Inst. Industrial Manufacturing Tech., Tokyo.
35. Uchino, K., and Nomura, S. (1983). *Ferroelectrics* **50**: 191.
36. Furuta, A., Oh, K. Y., and Uchino, K. (1992). *Sensors Mater.* **3**: 205.
37. Takahashi, S., Ochi, A., Yonezawa, M., Yano, T., Hamatsuki, T., and Fujui, I. (1993). *Ferroelectrics* **50**: 181.
38. Bauer, A., and Moller, F. (1994). "Proc. 4th Int'l Conf. New Actuators", p. 128.
39. Active Control Experts, Inc. (1996). Catalogue "PZT Quick Pack".
40. Sugawara, Y., Onitsuka, K., Yoshikawa, S., Xu, Q. C., R. Newnham, E., and Uchino, K. (1992). *J. Am. Ceram. Soc.* **75**: 996.
41. Goto, H., Imanaka, K., and Uchino, K. (1992). *Ultrasonic Technol.* **5**: 48.
42. Kanbe, N., Aoyagi, M., Hirose, S., and Tomikawa, Y. (1993). *J. Acoust. Soc. Jpn. (E)* **14**: 235.
43. Sugiyama, S., and Uchino, K. (1986). "Proc. Int'l. Symp. Appl. Ferroelectrics '86", p. 637, IEEE.
44. Kusakabe, C., Tomikawa, Y., and Takano, T. (1990). *IEEE Trans. UFFC* **37**: 551.
45. Ota, T., Uchikawa, T., and Mizutani, T. (1985). *Jpn. J. Appl. Phys.* **24** (Suppl. 24-3): 193.
46. Dorsey, J. T., Sutter, T. R., and Wu, K. C. (1992). "Proc. 3rd Int'l Conf. Adaptive Structures", p. 352.
47. Wada, B. (1993). JPL Document D-10659, p. 23.
48. Straub, F. K. (1996). *Smart Mater. Struct.* **5**: 1.
49. Chen, P. C., and Chopra, I. (1996). *Smart Mater. Struct.* **5**: 35.
50. Ohgoshi, A., and Nishigaki, S. (1981). *Ceramic Data Book '81*, p. 35, Tokyo: Inst. Industrial Manufacturing Technology.
51. Yano, T., Sato, E., Fukui, I., and Hori, S. (1989). "Proc. Int'l Symp. Soc. Information Display", p. 180.
52. Tanaka, Y. (1994). *Handbook on New Actuators for Precision Control*, p. 764. Fuji Technosystem.
53. Yokoya, Y. (1991). *Electron. Ceram.* **22**: 55.
54. Koster, M. P. (1994). "Proc. 4th Int'l Conf. New Actuators", Germany, p. 144.
55. Barth, H. V. (1973). *IBM Tech. Disclosure Bull.* **16**: 2263.
56. Lavrinenko, V. V., Vishnevski, S. S., and Kartashev, I. K. (1976). *Izvestiya Vysshikh Uchebnykh Zavedenii, Radioelektronica* **13**: 57.
57. Vasiliev, P. E. *et al.* (1979). UK Patent Application GB 2020857 A.

58. Sashida, T. (1982). *Oyo Butsuri* **51**: 713.
59. Kumada, A. (1985). *Jpn. J. Appl. Phys.* **24** (Suppl. 24–2): 739.
60. Koc, B., Bouchilloux, P., and Uchino, K. (2000). *IEEE Trans. UFFC* **47**: 836.
61. Fuda, Y., and Yoshida, T. (1994). *Ferroelectrics* **160**: 323.
62. Nakamura, K., Kurosawa, M., and Ueha, S. (1993). *Proc. Jpn. Acoustic Soc.* No.1-1-18, 917.
63. Uchino, K., Kato, K., and Tohda, M. (1988). *Ferroelectrics* **87**: 331.
64. Tomikawa, Y., Nishituka, T., Ogasawara, T., and Takano, T. (1989). *Sensors Mater.* **1**: 359.
65. Sashida, T. (1983). *Mech. Automation Jpn.* **15**: 31.
66. Ise, K. (1987). *J. Acoust. Soc. Jpn.* **43**: 184.
67. Kasuga, M., Satoh, T., Tsukada, N., Yamazaki, T., Ogawa, F., Suzuki, M., Horikoshi, I., and Itoh, T. (1991). *J. Soc. Precision Eng.* **57**: 63.
68. Cummings, J., and Stutts, D. (1994). Design for manufacturability of ceramic components, *Am. Ceram. Soc. Trans.*, p. 147.
69. Kumada, A. (1989). *Ultrasonic Technol.* **1**: 51.
70. Tomikawa, Y., and Takano, T. (1990). *Nikkei Mechanical* (Suppl.) 194.
71. Yoshida, T. (1989). "Proc. 2nd Memorial Symp. Solid Actuators of Japan: Ultra-precise Positioning Techniques and Solid Actuators for Them", p. 1.
72. Dong, S., Uchino, K., and Lim, L. C. (2000). IEEE Trans. UFFC.

AQ: Please update